

# Spectral and transport properties of a half-filled Anderson impurity coupled to phase-biased superconducting and metallic leads

Peter Zalom,<sup>1,\*</sup> Vladislav Pokorný,<sup>1,†</sup> and Tomáš Novotný<sup>2,‡</sup>

<sup>1</sup>*Institute of Physics, Czech Academy of Sciences,  
Na Slovance 2, CZ-18221 Praha 8, Czech Republic*

<sup>2</sup>*Department of Condensed Matter Physics, Faculty of Mathematics and Physics,  
Charles University, Ke Karlovu 5, CZ-12116 Praha 2, Czech Republic*

(Dated: September 30, 2021)

We derive and apply a general scheme for mapping a setup consisting of a half-filled single level quantum dot coupled to one normal metallic and two superconducting phase-biased leads onto an ordinary half-filled single impurity Anderson model with single modified tunneling density of states. The theory allows for the otherwise unfeasible application of the standard numerical renormalization group and enables to obtain phase-dependent local spectral properties as well as phase-dependent induced pairing and Josephson current. The resulting transport properties match well with the numerically exact continuous-time hybridization-expansion quantum Monte Carlo. For weakly coupled normal electrode, the spectral properties can be interpreted in terms of normal-electrode-broadened Andreev bound states with phase-dependent position analogous to the superconducting Anderson model, which coexist in the  $\pi$ -like phase with a Kondo peak whose phase-dependent Kondo temperature follows the form conjectured previously in Domański et al., Phys. Rev. B **95**, 045104 (2017).

## I. INTRODUCTION

Gradual advance in experimental techniques over the past decades allowed to study electronic transport in increasingly sophisticated nanoscale systems with various, competing correlations. A prototype experiment typically includes a strongly interacting mesoscopic system attached to a reservoir with well defined properties. In theory, the mesoscopic system is frequently described in terms of one or multiple quantum dots (QDs) in the Coulomb blockade regime while the reservoir consists of normal metallic and/or superconducting leads. Experimental realizations of such QDs include, for example, carbon nanotubes [1–9] or semiconductor nanowires [10–13].

The case of normal metallic electrodes attached to one QD can be modeled microscopically by the single impurity Anderson model (SIAM) which is one of the most understood models in the many-body physics [14]. Here, free conduction electrons of the reservoir can completely or partially screen the magnetic doublet of QD depending on the parameters under the study. When the screening is effective, an emergent Kondo singlet becomes the ground state of the system [14]. The Kondo singlet is a coherent many-body state composed of a screening cloud and QD states. It is specific due to its logarithmic energy scaling which can be fully understood only by applying renormalization group (RG) techniques [15–17] or at least effective renormalization schemes [18, 19].

Once superconducting correlations are considered in the reservoir, the electron transport is altered by the Andreev scattering on the interface between the leads and

QD [20–24], but it is still well described theoretically in terms of the Anderson impurity model with superconducting leads [25]. For purely superconducting reservoirs, both the theoretical [26, 27] and experimental [28] understanding is fairly complete. In particular, a sufficiently large gap depopulates electrons around the Fermi energy to such an extent that the screening cloud around the impurity becomes disrupted. The ground state of the system changes then from a singlet (effective screening at small sized gaps) to a doublet, which is an example of a impurity quantum phase transition (QPT). This so-called  $0$ - $\pi$  transition is accompanied by the reversal of the supercurrent, which is positive in the singlet and negative in the doublet phase [5, 10, 29]. At the transition, one also observes the crossing of the Andreev bound states (ABSs) at the Fermi energy.

Hybrid systems incorporating simultaneously normal as well as superconducting reservoirs, lead to even more intricate interplay of quantum correlation effects, where the understanding is limited both theoretically and experimentally [26]. In a simplest realization, one metallic and one superconducting lead have been studied experimentally in N-QD-S heterostructures [30, 31]. From the theoretical perspective, such problem is of only two-channel nature and thus well tractable by the numerical renormalization group (NRG) which offers unbiased insights and thus complements the purely numerical quantum Monte Carlo (QMC) simulations with reliable spectral properties [32]. However, having just one superconducting lead does not allow superconducting phase difference across the QD. Consequently, such systems lack any supercurrent flow and no interplay of Kondo and Josephson effects takes place. Thus, the more interesting scenario includes one normal and two phase-biased superconducting leads. The resulting three-terminal structure is, however, beyond the reach of standard NRG techniques since the corresponding discretized reservoir

\* zalomp@fzu.cz

† pokornyv@fzu.cz

‡ tno@karlov.mff.cuni.cz

model corresponds to three spin dependent and mutually interconnected hopping chains. The standard NRG scheme has thus been so far employed only to two channel problems [33, 34].

In the standard, computationally intractable approach to NRG, one would first discretize the bath of the three terminals. The resulting semi-infinite hopping chain would be then transformed via the Bogolyubov-Valatin transformation at each chain site. Subsequently, in the second step, particle-hole transformations on odd and even sites separately need to be carried out [33, 34]. The resulting Wilson chain would, however, consist of three mutually interconnected spin-polarized chains which is beyond the present computational power [32]. To circumvent the problem, one may apply a general procedure of Ref. [35] or introduce suitable unitary transformations to diagonalize the problem [36, 37]. The second approach has already been successfully applied to the hybrid normal-superconductor reservoir problem in the limit of infinite superconducting gap. Although, the authors of Refs. [36, 37] make explicit reference to Wilson chains corresponding to discretized versions of the model under the study, as shown in the present paper, it is possible to limit the transformations in the case of half-filling to just the local electrons of QD and map the infinite-gap model onto an ordinary asymmetric SIAM directly.

Generalizing the approach of Refs. [36, 37], we are able to treat the present general three-terminal problem at the half-filling with finite superconducting gap and map it onto a single impurity Anderson model of fermions with tunneling density of states (DOS) in the reservoir that corresponds to the standard one-channel-lead case tractable by NRG in the scheme of Ref. [38]. Since it is believed that such an approach is not feasible [39], we present the details of the transformation in Sec. II where also a detailed microscopic formulation of the problem is formulated. In Sec. III, we proceed to the  $\Delta \rightarrow \infty$  case treated previously in Refs. [36, 37] and show that their approach is in complete equivalence with the one presented here once half-filled case is considered. However, as opposed to Refs. [36, 37], no reference to NRG discretization scheme is required at the microscopic level. Finally in Sec. IV, the general three-terminal problem with finite superconducting gap is solved at the half-filling. To this end, the mapping of the finite-gap problem onto a single-channel SIAM with altered tunneling DOS is performed. Subsequently, standard NRG approach of Ref. [38] is employed utilizing the NRG Ljubljana code [40]. Using the corresponding backwards transformations, all spectral and transport properties of the original three-terminal setup are then determined. The most important conclusions are finally summarized in Sec. V. Technical calculations regarding the transformation of the interaction term in Sec. II and the effect of the finite band width are discussed in the Appendices A and B, respectively. The comparison with QMC is shown in the Appendix C.

## II. MAPPING ONTO SIAM-LIKE MODELS

### A. Microscopic formulation

The hybrid three-terminal setup consists of a mesoscopic system modeled as a usual Anderson magnetic impurity connected to one normal metallic and two superconducting electrodes. The superconducting electrodes follow the Bardeen-Cooper-Schrieffer (BCS) theory of conventional  $s$ -wave superconductivity. One of the BCS leads is then referred to as the left ( $L$ ) and the other as the right ( $R$ ) lead, see Fig. 1. They are considered to have arbitrary BCS phase parameters  $\varphi_L$  and  $\varphi_R$  but the same gap parameter  $\Delta_L = \Delta_R \equiv \Delta$ . The total Hamiltonian of the system is then the sum of the dot Hamiltonian  $H_d$ , the Hamiltonian of the normal lead  $H_N$ , two BCS Hamiltonians for superconducting leads  $H_L$  and  $H_R$ , and three tunneling Hamiltonians  $H_{T,\alpha}$  with  $\alpha \in \{N, L, R\}$  which connect each lead separately to the dot. The constituent Hamiltonians read as

$$H_d = \sum_{\sigma} \varepsilon_d d_{\sigma}^{\dagger} d_{\sigma} + U d_{\uparrow}^{\dagger} d_{\uparrow} d_{\downarrow}^{\dagger} d_{\downarrow}, \quad (1)$$

$$H_{\alpha} = \sum_{\mathbf{k}\sigma} \varepsilon_{\mathbf{k}\alpha} c_{\alpha\mathbf{k}\sigma}^{\dagger} c_{\alpha\mathbf{k}\sigma} - \Delta_{\alpha} \sum_{\mathbf{k}} \left( e^{i\varphi_{\alpha}} c_{\alpha\mathbf{k}\uparrow}^{\dagger} c_{\alpha-\mathbf{k}\downarrow}^{\dagger} + H.c. \right), \quad (2)$$

$$H_{T,\alpha} = \sum_{\alpha\mathbf{k}\sigma} \left( V_{\alpha\mathbf{k}}^* c_{\alpha\mathbf{k}\sigma}^{\dagger} d_{\sigma} + V_{\alpha\mathbf{k}} d_{\sigma}^{\dagger} c_{\alpha\mathbf{k}\sigma} \right), \quad (3)$$

where  $c_{\alpha\mathbf{k}\sigma}^{\dagger}$  creates an electron of spin  $\sigma$  and quasi-momentum  $\mathbf{k}$  in the lead  $\alpha$  while  $c_{\alpha\mathbf{k}\sigma}$  annihilates it. In analogy,  $d_{\sigma}^{\dagger}$  creates a dot electron of spin  $\sigma$  while  $d_{\sigma}$  annihilates it. The QD is characterized by the Coulomb repulsion  $U$  and the level energy  $\varepsilon_d$  which in the most general case is arbitrary but we will later concentrate only at  $\varepsilon_d = -U/2$ . The QD hybridizes with the leads via  $V_{\alpha\mathbf{k}}$  and the gap parameter vanishes in the normal lead, thus  $\Delta_N = 0$ .

To allow for an unbiased treatment of the Kondo and superconducting correlations on the same footing, RG techniques should be applied. However, in the basis of the  $d$  and  $c$  electrons, superconducting leads mix together the spin up and spin down electrons of the bath which requires to solve a general problem of three mutually interacting spin-polarized-bath channels. Applying the original numerical RG scheme [15] is therefore extremely demanding from the point of view of the computational time [32]. In general, multichannel problems pose a genuine challenge when applying NRG and have been tackled only quite recently within the interleaved formulation of the generalized Wilson chain [41].

Nevertheless, in the present case Hamiltonians of all three leads are quadratic because lead electrons are considered to be mutually non-interacting. Consequently, the lead electrons can be integrated out to obtain a genuine one channel impurity problem. To this end, it is ad-

vantageous to reformulate Eqs. (1)-(3) using the Nambu formalism.

### B. Hamiltonian in the Nambu basis

Nambu formalism represents a convenient way of rearranging Hamiltonians involving BCS superconductivity in a way where the lead electrons are all treated on the same footing. To this end, let us combine the spin up and spin down component of the corresponding fields describing the  $c$  electrons into spinors

$$C_{\alpha\mathbf{k}}^\dagger = \begin{pmatrix} c_{\alpha\mathbf{k}\uparrow}^\dagger, c_{\alpha-\mathbf{k}\downarrow} \end{pmatrix} \quad (4)$$

with  $\alpha \in \{N, L, R\}$ , while the spinor  $D$  of the dot electrons  $d$  is constructed in complete analogy as

$$D^\dagger = \begin{pmatrix} d_\uparrow^\dagger, d_\downarrow \end{pmatrix}. \quad (5)$$

The Hamiltonians (2) and (3) become then

$$H_\alpha = \sum_{\mathbf{k}} C_{\alpha\mathbf{k}}^\dagger \mathbb{E}_{\alpha\mathbf{k}} C_{\alpha\mathbf{k}}, \quad (6)$$

$$H_{T,\alpha} = \sum_{\mathbf{k}} D^\dagger \mathbb{V}_{\alpha\mathbf{k}} C_{\alpha\mathbf{k}} + C_{\alpha\mathbf{k}}^\dagger \mathbb{V}_{\alpha\mathbf{k}} D \quad (7)$$

with

$$\mathbb{E}_{\alpha\mathbf{k}} = \Delta_\alpha C_\alpha \sigma_x - \Delta_\alpha S_\alpha \sigma_y + \epsilon_{\mathbf{k}} \sigma_z, \quad (8)$$

$$\mathbb{V}_{\alpha\mathbf{k}} = V_{\alpha\mathbf{k}} \sigma_z, \quad (9)$$

where  $V_{\alpha\mathbf{k}}$  has been considered to be a real function only,  $\sigma_i$ ,  $i \in \{x, y, z\}$ , are Pauli matrices while  $C_\alpha \equiv \cos \varphi_\alpha$ ,  $S_\alpha \equiv \sin \varphi_\alpha$ . The blackboard bold typeface is from now on used to distinguish matrices from scalars.

Before applying the Nambu formalism to the Hamiltonian (1), let us first separate it into a quadratic part

$$\begin{aligned} H_{d,0} &= \sum_{\sigma} \varepsilon_d d_\sigma^\dagger d_\sigma + \frac{U}{2} D^\dagger (\sigma_x + \sigma_z) D \\ &= D^\dagger \mathbb{E}_d D \end{aligned} \quad (10)$$

with

$$\mathbb{E}_d = \frac{U}{2} \sigma_x + \left( \frac{U}{2} + \epsilon_d \right) \sigma_z \quad (11)$$

and a mixed quadratic and quartic interaction part

$$H_U = U d_\uparrow^\dagger d_\uparrow d_\downarrow^\dagger d_\downarrow - \frac{U}{2} D^\dagger (\sigma_x + \sigma_z) D. \quad (12)$$

The advantage of this non-standard partitioning will be discussed in Sec. II C.

Taking together, in the Nambu formalism the non-interacting quadratic part of the present problem spanned by the  $D$  and  $C$  spinors reads as

$$H_0 = H_{d,0} + \sum_{\alpha} (H_\alpha + H_{T,\alpha}) \quad (13)$$

while the modified interaction part  $H_U$  is given by Eq. (12).

### C. Bogolyubov-Valatin transformations in the space of local electrons

Let us now study the effect of unitary transformations  $\mathbb{T}$  and  $\tilde{\mathbb{T}}_\alpha$  onto the spinors  $D$  and  $C_\alpha$  respectively. We introduce the spinors  $W$  and  $\tilde{C}$  via

$$\mathbb{T}D \equiv W, \quad D^\dagger \mathbb{T}^\dagger \equiv W^\dagger, \quad (14)$$

$$\tilde{\mathbb{T}}_\alpha C_{\alpha\mathbf{k}} \equiv \tilde{C}_{\alpha\mathbf{k}}, \quad C_{\alpha\mathbf{k}}^\dagger \tilde{\mathbb{T}}_\alpha^\dagger \equiv \tilde{C}_{\alpha\mathbf{k}}^\dagger. \quad (15)$$

At this point, we consider no other constraints on the transformations  $\mathbb{T}$ ,  $\tilde{\mathbb{T}}_\alpha$  except of unitarity so that the many-body energy spectra of the problem remain the same in both spinor bases  $D$  and  $W$ . On the other hand, such transformations may crucially affect the form of the one-particle operators in the corresponding non-interacting Hamiltonians thus allowing for computationally more suitable non-interacting Green functions and/or self-energy contributions from the integrable degrees of freedom for the problem under the study.

The effect of the transformations  $\mathbb{T}$  and  $\tilde{\mathbb{T}}_\alpha$  on the quadratic part  $H_{d,0}$  reads as

$$H_{d,0} = W^\dagger (\mathbb{T} \mathbb{E}_d \mathbb{T}^\dagger) W, \quad (16)$$

while the tunneling Hamiltonians change as

$$\begin{aligned} H_{T,\alpha} &= \sum_{\mathbf{k}} W^\dagger \left( \mathbb{T} \mathbb{V}_{\alpha\mathbf{k}} \tilde{\mathbb{T}}_\alpha^\dagger \right) \tilde{C}_{\alpha\mathbf{k}} \\ &\quad + \sum_{\mathbf{k}} \tilde{C}_{\alpha\mathbf{k}}^\dagger \left( \tilde{\mathbb{T}}_\alpha \mathbb{V}_{\alpha\mathbf{k}} \mathbb{T}^\dagger \right) W. \end{aligned} \quad (17)$$

The kinetic Hamiltonians are affected only by the transformations  $\tilde{\mathbb{T}}_\alpha$  as they involve no operators of the local electrons:

$$H_\alpha = \sum_{\mathbf{k}} \tilde{C}_{\alpha\mathbf{k}}^\dagger \left( \tilde{\mathbb{T}}_\alpha \mathbb{E}_{\alpha\mathbf{k}} \tilde{\mathbb{T}}_\alpha^\dagger \right) \tilde{C}_{\alpha\mathbf{k}}. \quad (18)$$

Since the non-interacting ( $U = 0$ ) Hamiltonian is quadratic we can easily obtain the retarded Green function  $\mathbb{G}_0^W(\omega^+)$  which corresponds to the  $W$  spinors. Employing the equation of motion technique for the Green functions in an exact analogy to Ref. [42], we introduce an infinite-dimensional vector

$$\Psi^\dagger = (W^\dagger, \tilde{C}_{N\mathbf{k}}^\dagger, \tilde{C}_{L\mathbf{k}}^\dagger, \tilde{C}_{R\mathbf{k}}^\dagger), \quad (19)$$

where  $\Psi$  is its Hermitian conjugate and the spinors  $\tilde{C}_{\alpha\mathbf{k}}^\dagger$  are understood to be repeated in  $\Psi^\dagger$  for all possible momenta of lead electrons. This allows us to rearrange the non-interacting Hamiltonian as

$$H_0 = \Psi^\dagger \mathbb{E}^W \Psi, \quad (20)$$

with

$$\mathbb{E}^W = \begin{pmatrix} \mathbb{T} \mathbb{E}_d \mathbb{T}^\dagger & \mathbb{T} \mathbb{V}_{N\mathbf{k}} \tilde{\mathbb{T}}_N^\dagger & \mathbb{T} \mathbb{V}_{L\mathbf{k}} \tilde{\mathbb{T}}_L^\dagger & \mathbb{T} \mathbb{V}_{R\mathbf{k}} \tilde{\mathbb{T}}_R^\dagger \\ \tilde{\mathbb{T}}_N \mathbb{V}_{L\mathbf{k}} \mathbb{T}^\dagger & \tilde{\mathbb{T}}_N \mathbb{E}_{N\mathbf{k}} \tilde{\mathbb{T}}_N^\dagger & 0 & 0 \\ \tilde{\mathbb{T}}_L \mathbb{V}_{L\mathbf{k}} \mathbb{T}^\dagger & 0 & \tilde{\mathbb{T}}_L \mathbb{E}_{L\mathbf{k}} \tilde{\mathbb{T}}_L^\dagger & 0 \\ \tilde{\mathbb{T}}_R \mathbb{V}_{R\mathbf{k}} \mathbb{T}^\dagger & 0 & 0 & \tilde{\mathbb{T}}_R \mathbb{E}_{R\mathbf{k}} \tilde{\mathbb{T}}_R^\dagger \end{pmatrix}, \quad (21)$$

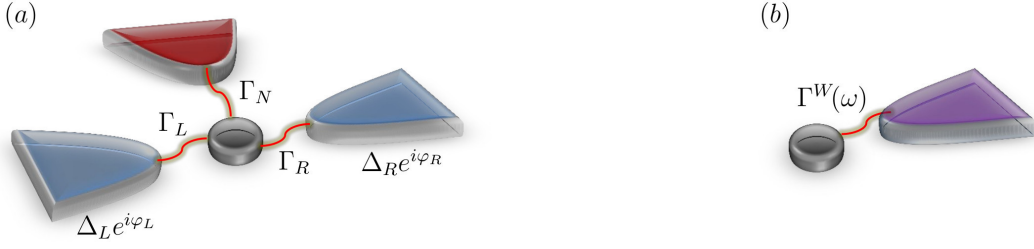


FIG. 1. (a) Scheme of Y-shaped three-terminal junction where a QD (black disc) couples via the hybridization strength  $\Gamma_N$  to one normal electrode (red pointed teardrop) and left (L) and the right (R) superconducting electrode (blue pointed teardrop) which are phase-biased by  $\varphi = \varphi_L - \varphi_R$ . The BCS leads hybridize with quantum dot with strengths  $\Gamma_L$  and  $\Gamma_R$ , respectively, and are considered here as having the same BCS gap parameter  $\Delta_L = \Delta_R \equiv \Delta$ . (b) Equivalent scheme consisting of one-terminal reservoir containing Bogolyubov-like quasiparticles (purple pointed teardrop) which are hybridized with the QD via a structured hybridization function  $\Gamma^W(\omega)$ . In Sec. II C we show that by employing  $\Gamma^W(\omega)$  according to Eq. (30) the schemes (a) and (b) may be in terms of spectral properties mapped onto each other at the half-filling. To obtain transport properties corresponding to the Y shape geometry of panel (a) transformations according to Sec. IV C are required.

where the upper index  $W$  was introduced to clearly distinguish the underlying spinor basis  $W$  for the formulation of the infinite-dimensional matrix  $\mathbb{E}^W$ .

In general, the non-interacting problem can be solved by finding the retarded Green function  $\mathbb{G}_0(\omega^+)$  where  $\omega^+ \equiv \omega + i\eta$  while  $\omega$  is a real frequency and  $\eta$  is an infinitesimally small positive number. To this end, standard equation of motion technique formulated in the matrix form requires one to solve the resolvent equation  $\mathbb{G}_0(\omega^+) = (\omega^+ \mathbb{1} - \mathbb{H}_0)^{-1}$  with  $\mathbb{1}$  being the unit matrix. However, for the present problem we only need to obtain the solution for the local Green function of the dot electrons which corresponds the left upper  $2 \times 2$  block of expression (21). Employing the partitioning scheme of Ref. [42], we obtain the local retarded Green function  $\mathbb{G}_0^W(\omega^+)$  in the spinor basis  $W$  directly as

$$\mathbb{G}_0^W(\omega^+) = (\omega^+ \mathbb{1} - \mathbb{T} \mathbb{E}_d \mathbb{T}^\dagger - \mathbb{T} \Sigma^D \mathbb{T}^\dagger)^{-1} \quad (22)$$

with

$$\begin{aligned} \Sigma^D(\omega^+) &= \sum_{\alpha \mathbf{k}} \mathbb{V}_{\alpha \mathbf{k}} \tilde{\mathbb{T}}_\alpha^\dagger (\omega^+ \mathbb{1} - \tilde{\mathbb{T}}_\alpha \mathbb{E}_{\alpha \mathbf{k}} \tilde{\mathbb{T}}_\alpha^\dagger)^{-1} \tilde{\mathbb{T}}_\alpha \mathbb{V}_{\alpha \mathbf{k}} \\ &= \sum_{\alpha \mathbf{k}} \mathbb{V}_{\alpha \mathbf{k}} (\omega^+ \mathbb{1} - \mathbb{E}_{\alpha \mathbf{k}})^{-1} \mathbb{V}_{\alpha \mathbf{k}}, \end{aligned} \quad (23)$$

which thus represents the self-energy contribution from the leads expressed with respect to the spinor basis  $D$  (as denoted by the upper index  $D$ ). Moreover, one may also obtain the self-energy contribution  $\Sigma^W$  as

$$\Sigma^W(\omega^+) = \mathbb{T} \Sigma^D(\omega^+) \mathbb{T}^\dagger, \quad (24)$$

which not only defines  $\Sigma^W(\omega^+)$ , but also gives us the transformation rule to easily interchange the spinor bases  $D$  and  $W$  when required. By exploiting the unitarity of  $\mathbb{T}$ , we may also extract an analogous transformation rule for the non-interacting retarded Green functions

$$\mathbb{G}_0^W(\omega^+) = \mathbb{T} (\omega^+ \mathbb{1} - \mathbb{E}_d - \Sigma^D)^{-1} \mathbb{T}^\dagger = \mathbb{T} \mathbb{G}_0^D(\omega^+) \mathbb{T}^\dagger \quad (25)$$

which yields the transformation rule as well as the definition of the non-interacting ( $U = 0$ ) retarded Green function with respect to the spinor basis  $D$ . Clearly, in both bases the effect of the leads is fully integrated out and only enters the  $\mathbb{G}_0^W(\omega^+)$  and  $\mathbb{G}_0^D(\omega^+)$  via the corresponding self-energy contributions  $\Sigma^W(\omega^+)$  and  $\Sigma^D(\omega^+)$ , respectively. Green function as well as the self-energy contributions in different bases relate to each other via the local dot transformation  $\mathbb{T}$  since the transformations  $\tilde{\mathbb{T}}_\alpha$  are canceled out in Eqs. (24) and (25).

It is now our aim to construct a suitable transformation  $\mathbb{T}$ , so that the self-energy contribution  $\Sigma^W$  is diagonal. To this end, we first perform all summations in Eq. (23), which is a quite straightforward with details given in the Appendix B. The resulting expression for  $\Sigma^D(\omega^+)$  has the following matrix structure:

$$\Sigma^D(\omega^+) = \Sigma_N^D(\omega) \mathbb{1} + \Sigma_A^D(\omega) \sigma_x, \quad (26)$$

where  $\Sigma_N^D(\omega)$  and  $\Sigma_A^D(\omega)$  are functions of frequency with a for now unimportant form which is given in the Appendix B. We insert now  $\Sigma^D(\omega^+)$  back into Eq. (25) to obtain the matrix structure of  $(\mathbb{G}_0^D)^{-1}$ . We first concentrate exclusively on the half-filled case where  $(\mathbb{G}_0^D)^{-1}$  has a much simpler structure. Afterwards, the more general  $\varepsilon_d \neq -U/2$  case is inspected.

At the half-filling the diagonal part of  $(\mathbb{G}_0^D)^{-1}$  is only proportional to the unit matrix  $\mathbb{1}$  which remains unaltered under unitary transformation. On the other hand, the off-diagonal parts of  $\Sigma^D$  and  $\mathbb{E}_d$  are both proportional to  $\sigma_x$  and may thus be simultaneously diagonalized by enforcing the condition  $\mathbb{T} \sigma_x \mathbb{T}^\dagger = \pm \sigma_z$  onto the transformation  $\mathbb{T}$ . The resulting non-interacting Green function  $\mathbb{G}_0^W$  is then also diagonal as intended. Each sign option of the condition  $\mathbb{T} \sigma_x \mathbb{T}^\dagger = \pm \sigma_z$ , is solved by two linearly independent transformations which we denote  $\mathbb{T}_1^\pm$  and  $\mathbb{T}_2^\pm$  with the given superscript indicating the sign of  $\sigma_z$  in the

condition. Explicitly, we obtain

$$\begin{aligned}\mathbb{T}_1^\pm &= \frac{1}{\sqrt{2}}(\sigma_x \pm \sigma_z), \\ \mathbb{T}_2^\pm &= \frac{1}{\sqrt{2}}(\mathbb{1} \pm i\sigma_y).\end{aligned}\quad (27)$$

Note, that all transformations fulfill  $\mathbb{T}^\dagger = \mathbb{T}^{-1} = \mathbb{T}$  and are of Bogolyubov-Valatin type but unlike in BCS superconductors they do not involve momentum or frequency dependence.

Now it also becomes obvious, why the half-filled case was selected first. Generalizing the previous approach to  $\varepsilon_d \neq -U/2$  changes the matrix structure of  $(\mathbb{G}_0^D)^{-1}$  considerably by adding an extra diagonal term proportional to  $(\varepsilon_d + U/2)\sigma_z$ . Diagonalizing  $(\mathbb{G}_0^D)^{-1}$  by  $\mathbb{T}$  would now require to simultaneously fulfill not only  $\mathbb{T}\sigma_x\mathbb{T}^\dagger = \pm\sigma_x$  but also  $\mathbb{T}\sigma_z\mathbb{T}^\dagger = \pm\sigma_z$  or  $\mathbb{T}\sigma_z\mathbb{T}^\dagger = \pm\mathbb{1}$ . Neither of the two combined conditions is however solvable. Consequently, outside of the half-filled case there exists no unitary transformation to diagonalize  $(\mathbb{G}_0^D)^{-1}$ . For example, applying  $\mathbb{T}$  in the form of Eq. (27) away from the half-filling rotates the superconducting terms onto the diagonal elements of  $(\mathbb{G}_0^W)^{-1}$  which is however traded off for rotating the originally diagonal terms proportional to  $(\varepsilon_d + U/2)\sigma_z$  into off-diagonal terms proportional to  $(\varepsilon_d + U/2)\sigma_x$ . From now on, we therefore concentrate *exclusively on the half-filled case*.

Although, for the non-interacting ( $U = 0$ ) half-filled case the corresponding Green function can be diagonalized by transformations (27), in the end, in the full interacting case the action of transformations (27) on the interaction part  $H_U$  needs to be considered. As shown in the Appendix A, using the interaction term mixed of quadratic and quartic terms according to Eq. (12) allows to obtain the Hubbard interaction term when the transformation  $\mathbb{T}_1^-$  is used. Explicitly:

$$H_U = U w_\uparrow^\dagger w_\uparrow w_\downarrow^\dagger w_\downarrow, \quad (28)$$

The remaining options for  $\mathbb{T}$  produce all an extra quadratic terms in  $H_U$  which is proportional to  $\sigma_x$ , thus spoiling the diagonal form of  $\mathbb{G}_0^W(\omega^+)$ . We thus select the transformation  $\mathbb{T}_1^-$  in what follows and denote it as  $\mathbb{T} \equiv \mathbb{T}_1^-$ . Nevertheless, we stress that the remaining choices would also be possible when different partitionings of the full Hamiltonian are considered. Moreover, the transformation  $\mathbb{T}_2^+$  fully corresponds to the transformation used in the standard NRG treatments of magnetic impurities coupled to superconducting reservoirs (see Refs. [33, 34] for more detail) while  $\mathbb{T}_1^+$  relates to the transformations applied in the Refs. [36, 37] to solve the  $\Delta \rightarrow \infty$  limit of the present model. However, in all of the aforementioned references, even at the half-filling the lead transformations corresponding to  $\mathbb{T}_\alpha$  are explicitly performed within the applied NRG algorithms.

Since the resulting  $\mathbb{G}_0^W(\omega^+)$  is proportional to  $\sigma_z$ , one may actually drop the Nambu formalism and employ directly the  $w_\uparrow^\dagger$  and  $w_\downarrow^\dagger$  fields which constitute the  $W$  spinor.

In such a case, we obtain:

$$G_{0\uparrow}^W(\omega^+) = G_{0\downarrow}^W(\omega^+) = \frac{1}{\omega + U/2 - \Sigma^W(\omega)}, \quad (29)$$

and the independence of Green functions of the spin index of the field  $w$  becomes explicit. Assuming the momentum-independent hybridizations  $V_{\alpha\mathbf{k}} \equiv V_\alpha$ , the calculation of  $\Sigma^W(\omega)$  can be performed for arbitrary band-width as shown in the Appendix B. In the limit of infinitely wide band, it takes the following form

$$\begin{aligned}\Sigma^W(\omega^+) &= -i\frac{\Gamma_N}{2} - \Gamma_S \left[ \frac{i \operatorname{sgn}(\omega)}{\sqrt{\omega^2 - \Delta^2}} \Theta(\omega^2 - \Delta^2) \right. \\ &\quad \left. + \frac{\Theta(\Delta^2 - \omega^2)}{\sqrt{\Delta^2 - \omega^2}} \right] \left( \omega + \Delta \cos \frac{\varphi}{2} \right),\end{aligned}\quad (30)$$

where  $\Theta$  is the Heaviside step function and  $\Gamma_N \equiv \pi\rho_0 V_N$  and  $\Gamma_S \equiv \pi\rho_0 V_S$  with  $\rho_0$  being the constant DOS of the band and  $V_S = V_L = V_R$ . As shown in Ref. [43], the  $V_L \neq V_R$  case can be directly obtained from the symmetric scenario of  $V_L = V_R$  introduced explicitly above. The imaginary part of Eq. (30) is traditionally referred to as the hybridization function, see also Sec. IV A, while the real part is connected to the imaginary one via Kramers-Kronig relations.

Taking together, the unitary transformation  $\mathbb{T}$  allows to map the original non-diagonal model expressed via  $D$  spinor onto a model described in terms of Bogolyubov-type quasiparticles  $w_\sigma$  coupled to a single normal lead which has an altered tunneling DOS due to the frequency-dependent self-energy  $\Sigma^W(\omega)$ . Moreover, the Bogolyubov quasiparticles  $w_\sigma$  interact locally via the ordinary Hubbard interaction term. This allows us to redefine the three-terminal setup as one-channel-lead problem similar to the ordinary SIAM and apply NRG in a straightforward way as described in Ref. [38]. This way, all spectral properties in the spinor basis  $W$  can be obtained.

Although the normal spectral function  $A_{\sigma N}^W(\omega)$  and the trivially vanishing anomalous spectral function  $A_{\sigma A}^W(\omega)$  in the basis of the  $w$  fields can be determined, in the end, we need to transform back to the original basis of the  $d$  electrons. Therefore, one needs to relate the Green functions and their corresponding spectral functions between both bases. Since the unitary transformation  $\mathbb{T}$  mixes the original  $d_\sigma$  and  $d_\sigma^\dagger$  fields only in a linear way, the corresponding normal Green function  $G_{\sigma N}^D$  and the corresponding anomalous Green function  $G_{\sigma A}^D$  in the basis of the  $d$  electrons are given by

$$G_{\sigma N}^D(\omega^+) = \frac{1}{2} [G_{\sigma N}^W(\omega^+) - G_{\sigma N}^W(-\omega^+)], \quad (31)$$

$$G_{\sigma A}^D(\omega^+) = \frac{1}{2} [G_{\sigma N}^W(\omega^+) + G_{\sigma N}^W(-\omega^+)], \quad (32)$$

where  $-\omega^+ \equiv -\omega - i\eta$ . Recall that  $G_\sigma^W(\omega^+) = G_\sigma^{W*}(\omega^-)$  with  $\omega^- = \omega - i\eta$  and the imaginary part of the Green function equals the spectral function up to a multiplicative prefactor  $-1/\pi$ . Therefore, we can directly construct

the normal spectral function  $A_{\sigma N}^D(\omega)$  and the anomalous spectral function  $A_{\sigma A}^D(\omega)$  in the  $d$  basis in the  $d$  basis using

$$A_{\sigma N}^D(\omega) = \frac{1}{2} [A_{\sigma N}^W(\omega) + A_{\sigma N}^W(-\omega)], \quad (33)$$

$$A_{\sigma A}^D(\omega) = \frac{1}{2} [A_{\sigma N}^W(\omega) - A_{\sigma N}^W(-\omega)]. \quad (34)$$

We will often refer to the backwards transformations of the normal spectral and anomalous function as symmetrization and antisymmetrization, respectively.

### III. $\Delta \rightarrow \infty$ CASE

The  $\Delta \rightarrow \infty$  case of the present model is already quite well understood with a general phase-dependent NRG solution given in Refs. [32, 36, 37]. Interestingly, in Refs. [36, 37] the authors have mapped the problem onto the standard asymmetric SIAM with constant tunneling DOS by employing similar Bogolyubov-Valatin transformations as discussed above. However, instead applying the transformations on the level of the Hamiltonian, they transform the Wilson chain corresponding to the discretized version of the  $\Delta \rightarrow \infty$  model. Such a procedure however requires not only the  $\mathbb{T}$  transformation of the dot electrons but also an analog of the  $\mathbb{T}_\alpha$  transformation of the leads which is applied to each site of the Wilson chain representing the lead electron contributions. Unnoticed by the authors of [36, 37], at the half-filling only the transformation  $\mathbb{T}$  is, however, explicitly required which we will now show. To this end, we briefly review the most crucial points made in Refs. [36, 37]. The  $\Delta \rightarrow \infty$  Hamiltonian simplifies to

$$H_{\Delta \rightarrow \infty} = H_{d,0} + H_U + H_N + H_{T,N} - \Delta_d(\varphi) (d_\uparrow^\dagger d_\downarrow^\dagger + d_\downarrow d_\uparrow), \quad (35)$$

where  $\Delta_d(\varphi) \equiv \Gamma_S \cos(\varphi/2)$  and  $H_N$ ,  $H_{d,0}$ ,  $H_{T,N}$  follow our previous notations and the authors have applied their approach to arbitrary values of  $\varepsilon_d$ . Obviously, the effective Hamiltonian is just of the one-channel-lead nature. However, the BCS effects are manifested by non-zero off-diagonal terms which cannot be treated directly by the original NRG algorithm [15]. In general, when off-diagonal terms emerge, as for example in the superconducting Anderson model (SCIAM), the construction of the Wilson chain requires to implement Bogolyubov-Valatin transformation to each site of the Wilson chain which is then followed by particle-hole transformations to each of the site except of the initial one. Such a series of transformations ensures then the diagonality of the emerging Wilson chain [33]. Due to the presence of the off-diagonal terms, a similar approach is then also applied for the  $\Delta \rightarrow \infty$  case [36, 37]. In detail, the logarithmically discretized version of  $\Delta \rightarrow \infty$  model gives rise to a semi-infinite Wilson hopping chain with the first node populated by the local  $d_\sigma$  electrons ( $\sigma \in \{\uparrow, \downarrow\}$ ) of

the QD and remaining sites labeled by  $i \in N$  and populated by fermions  $c_{i\sigma}$  which represent the bath degrees of freedom. In Refs. [36, 37], each site of the Wilson chain is then rotated using unitary transformation  $O_\Theta$  given by

$$O_\Theta = \begin{pmatrix} \cos \frac{\Theta}{2} & -\sin \frac{\Theta}{2} \\ \sin \frac{\Theta}{2} & \cos \frac{\Theta}{2} \end{pmatrix}, \quad (36)$$

with

$$\cos \frac{\Theta}{2} = \sqrt{\frac{1}{2} \left( 1 + \frac{\tilde{\varepsilon}_d}{\sqrt{\varepsilon_d^2 + \Delta_d^2}} \right)}, \quad (37)$$

$$\sin \frac{\Theta}{2} = \sqrt{\frac{1}{2} \left( 1 - \frac{\tilde{\varepsilon}_d}{\sqrt{\varepsilon_d^2 + \Delta_d^2}} \right)}, \quad (38)$$

which acts on the Nambu spinors of the given site of the Wilson chain,  $\delta = \sqrt{\varepsilon_d^2 + \Delta_d^2}$  and  $\tilde{\varepsilon}_d = \varepsilon_d + U/2$ . The factor  $\delta$  is later shown to correspond to the particle-hole asymmetry factor of the ordinary SIAM with constant tunneling DOS. For example, the  $D$  spinor of the first site of the Wilson chain transforms as

$$O_\Theta D = O_\Theta \begin{pmatrix} d_\uparrow \\ d_\downarrow \end{pmatrix} = \begin{pmatrix} w_\uparrow \\ w_\downarrow \end{pmatrix} \equiv W, \quad (39)$$

where  $W$  follows the notation of the previous section. Afterwards, all sites corresponding to the lead electrons (indexed by  $i$ ) are subjected to additional particle-hole transformations which are required to transform away the off-diagonal BCS terms in the Wilson hopping chain. Only then a semi-infinite chain feasible for standard NRG algorithms is constructed. The resulting coefficients of the semi-infinite Wilson chain are then noticed to be identical to those of the ordinary asymmetric SIAM and because of the Hausholder transformation [36, 37] equivalence of the  $\Delta \rightarrow \infty$  model to the asymmetric SIAM is finally noticed even at the microscopic level [36, 37]. We stress that the findings in Refs. [36, 37] hold at arbitrary filling.

However, once only the half-filling is considered, the unitary transformation  $O_\Theta$  may be restricted to act only in the space of local electrons while the transformations on the additional sites turn out to be merely a technical tool required if NRG-based discretizations are introduced before lead electrons are transformed accordingly. The proof is completely analogous to that of the finite-gap half-filled problem discussed above. We thus skip the details and discuss only the crucial steps.

We first notice, that the half-filled case in Refs. [36, 37], i.e.  $\tilde{\varepsilon}_d = \varepsilon_d + U/2 = 0$ , corresponds to  $\Theta = \pi/2$  for which the  $O_\Theta$  transformation becomes the  $\mathbb{T}_2^+$  transformation found previously for the general finite-gap model. Furthermore, the three-terminal structure of the leads enters the QD equation of motion only via the corresponding self-energy contribution, which for  $\Delta \rightarrow \infty$  is purely imaginary and proportional to the  $2 \times 2$  unit matrix as seen in the  $d$  basis of the local electrons. Thus, its form is

invariant under any unitary transformation. Explicitly:

$$\Sigma_N^D(\omega) = \Sigma_N^W(\omega) = -i\Gamma_N \mathbb{1}. \quad (40)$$

On the other hand, the off-diagonal parts of the dot Hamiltonian turn out to have a more intricate form. Performing then the same partitioning of the Hamiltonian as in Eqs. (10) and (12), we may apply the transformation  $O_{\pi/2}$  and transform the non-interacting part of the dot Hamiltonian into a diagonal form

$$H_{d,0} = W^\dagger \begin{pmatrix} \delta - \frac{U}{2} & 0 \\ 0 & -\delta + \frac{U}{2} \end{pmatrix} W. \quad (41)$$

Applying then the transformation  $O_{\pi/2}$  to the interaction term gives us subsequently the Hubbard repulsion term typical for SIAM. Consequently, at the half-filling transformation (39) maps the  $\Delta \rightarrow \infty$  model onto a general asymmetric SIAM with the particle-hole asymmetry related to the phase difference  $\varphi$  which remained unnoticed by the authors of Refs. [36, 37]. Applying the NRG algorithm according to Ref. [38] to the diagonal formulation of the  $\Delta \rightarrow \infty$  gives Wilson chain coefficients which are the same as those obtained by Refs. [36, 37]. The resulting spectral and transport properties are therefore the same and we review these only briefly below.

Before proceeding further, let us first clarify the role of the QD filling in the transformation procedures. Clearly, the transformations  $\mathbb{T}$  derived in this paper have been designed to work exclusively at the half-filling and fail to diagonalize the finite  $\Delta$  as well as the  $\Delta \rightarrow \infty$  case away from the half-filling. On the other hand, the transformation  $O_\Theta$  given by Eq. (39) and accompanied by corresponding particle-hole transformations of the Wilson chain diagonalizes only the  $\Delta \rightarrow \infty$  model but at an arbitrary filling. Nevertheless, at the half-filling  $O_\Theta$  is actually exactly the  $\mathbb{T}_2^+$  transformation which under proper choice of partitioning of the Hamiltonian allows to map even the finite-gap problem at the half-filling onto a simple SIAM. However, even for the  $\Delta \rightarrow \infty$  model the  $O_\Theta$  nor any other unitary transformation of the dot electrons is sufficient to solely diagonalize the problem away from the half-filling. This regarding, it is important to notice that the off-diagonal self-energy contribution of the hybrid reservoir of normal and superconducting electrons is proportional to  $\sigma_x$  in the basis of the  $d$  fields. Such contributions transform under  $O_\Theta$  as

$$O_\Theta^\dagger \begin{pmatrix} 0 & 1 \\ 1 & 0 \end{pmatrix} O_\Theta = \begin{pmatrix} \sin \Theta & \cos \Theta \\ \cos \Theta & -\sin \Theta \end{pmatrix} \quad (42)$$

and become diagonal only at the half-filling in complete analogy to the finite-gap model discussed above.

Since both transformations  $\mathbb{T}$  and  $O_\Theta$  accomplish the same for the  $\Delta \rightarrow \infty$  model at the half filling, we will briefly discuss the results and interpretations obtained via the transformation  $\mathbb{T}$  while all details on transport properties can be found in Refs. [36, 37]. The transformation  $\mathbb{T}$  maps the  $H_{\Delta \rightarrow \infty}$  Hamiltonian onto that of an

ordinary particle-hole asymmetric SIAM with the asymmetry parameter  $\delta = \Gamma_S \cos(\varphi/2)$ . This opens up an easy and efficient way of understanding the hybrid reservoir case just within the well known asymmetric SIAM [44]. To this end, one only needs the spectral function  $A_N^W(\omega)$  of the asymmetric SIAM with the asymmetry parameter  $\delta$  matching the parameters of the  $\Delta \rightarrow \infty$  case. Then, symmetrization procedure (33) is applied to obtain the normal spectral function  $A_N^D(\omega)$  of the three-terminal  $\Delta \rightarrow \infty$  model in the original basis of the  $d$  fields. For the anomalous functions (subscript  $A$ ) one proceeds analogically by antisymmetrization (34).

In Fig. 2, we present the spectral functions of the asymmetric SIAM for selected values of  $\delta$  (see the top row of panels) which have been obtained using the open source NRG Ljubljana code [40] in the one-channel mode with intertwined  $z$ -discretization [45] with  $z = n/10$ ,  $n \in \{0, \dots, 10\}$ . The middle row of panels shows the normal spectral functions of the  $\Delta \rightarrow \infty$  model obtained by the symmetrization of those from the top row. In the bottom row, the anomalous spectral functions of the  $\Delta \rightarrow \infty$  model are presented. Panels in the same columns correspond to each other via the relation  $\delta = \Gamma_S \cos(\varphi/2)$  and are ordered from left to right with the increasing phase difference  $\varphi$  and thus decreasing asymmetry parameter  $\delta$  of the underlying SIAM. The particle-hole symmetric case of the effective SIAM is then realized at  $\varphi = \pi$ . The mapping  $\mathbb{T}$  makes thus obvious that the competition between the Kondo and superconducting correlations, as explicitly seen in the basis of the  $d$  fields, simplifies into the ordinary Kondo physics away from the half-filling once the basis of the  $w$  fields is used.

Let us now discuss the consequences in more detail. In the basis of the  $w$  fields the particle-hole symmetry at  $\varphi = \pi$  manifests itself via the appearance of an ordinary Kondo resonance at the Fermi energy in the spectral function  $A_N^W(\omega)$ . Additionally, two satellite Hubbard peaks emerge at approximately  $\pm U/2$  (see the last column of panels in Fig. 2). Symmetrization (33) does not alter the shape of the normal spectral function which remains the same in both bases. In other words, in the  $\varphi = \pi$  case, Josephson and other superconducting effects do not disrupt Kondo correlations, which is a trivial result already visible from the effective Hamiltonian (35).

However, decreasing the phase difference  $\varphi$ , while keeping parameters  $U$ ,  $\Delta$ ,  $\Gamma_N$  and  $\Gamma_S$  constant, drives the effective system away from its particle-hole symmetric point with the asymmetry factor  $\delta$  of the underlying asymmetric SIAM increasing due to  $\delta = \Gamma_S \cos(\varphi/2)$ . Looking at the top row of panels in Fig. 2 in the direction of decreasing  $\varphi$  (from right to left), we observe the central peak corresponding to the Kondo resonance at  $\varphi = \pi$  shifting gradually away from the Fermi energy which is accompanied by its gradual broadening and mild decrease of its height [46]. When the particle-hole asymmetry in the basis of the  $w$  fields is relatively small, corresponding to  $\delta = 2.5$  for model parameters used in Fig. 2, the off-central movement of the peak does not

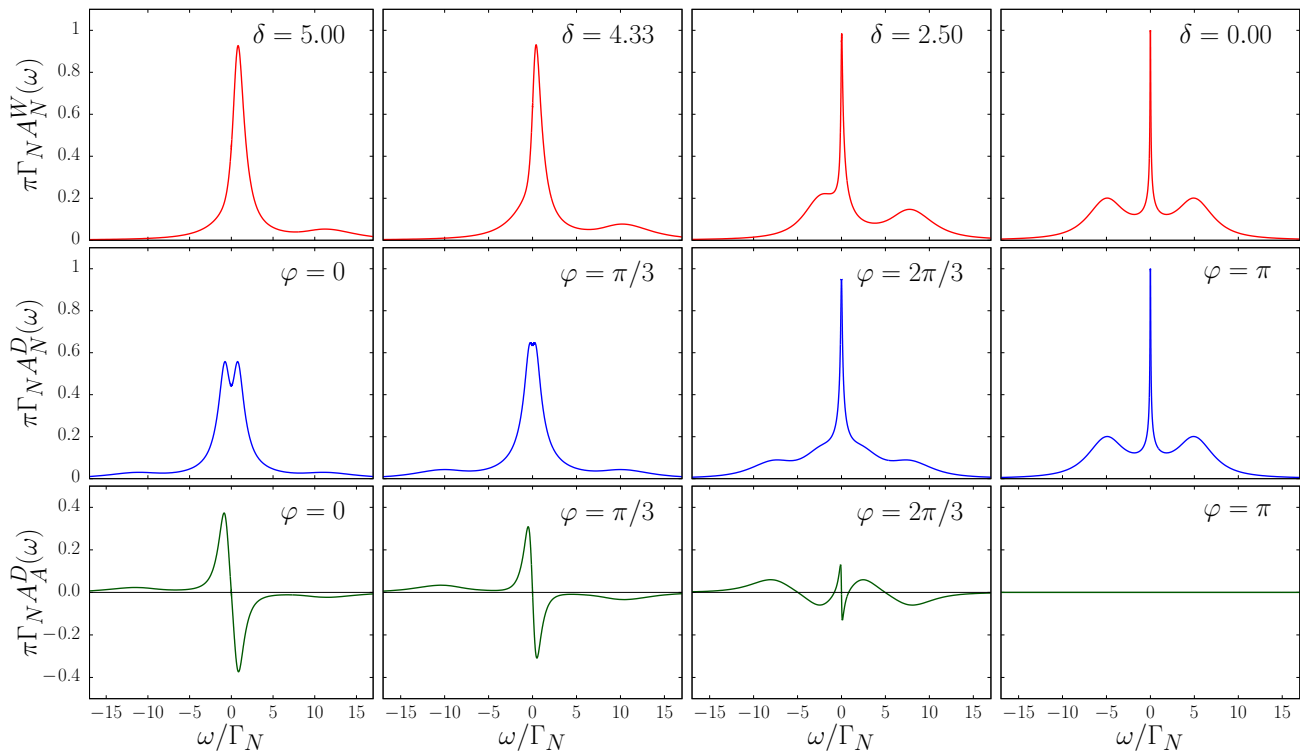


FIG. 2. The top row of panels shows the normal spectral functions for the asymmetric SIAM with  $U/\Gamma_N = 5$  in the direction of decreasing asymmetry parameter  $\delta$ . According to Eqs. (40) and (41), the top row spectral functions also correspond to the spectral functions  $A_N^W(\omega)$  of the  $\Delta \rightarrow \infty$  model expressed in the basis of the  $w$  fields when  $U$  and  $\Gamma_N$  are the same and  $\delta = \Gamma_s \cos(\varphi/2)$ . The middle row of panels shows the normal spectral functions  $A_N^D(\omega)$  of the  $\Delta \rightarrow \infty$  model in the basis of the  $d$  fields obtained by symmetrization (33) of  $A_N^W(\omega)$  corresponding to the top row. The bottom row shows the anomalous spectral function  $A_A^D(\omega)$  of the  $\Delta \rightarrow \infty$  model in the basis of the  $d$  fields obtained by antisymmetrization (34) of the top row.

overcome its broadening. Consequently, performing symmetrization operation (33) to obtain  $A_N^D(\omega)$  makes the central peak broader but still singly-peaked at the Fermi energy. However, decreasing the angle  $\varphi$  further increases the asymmetry parameter of the underlying asymmetric SIAM even more, which results in a very strong decentralization of the Kondo-like peak. The broadening is then not sufficient to overcome the shift and symmetrization (33) leads to a split central peak in the  $d$  basis (see the  $\delta = 4.33$  and  $\delta = 5.0$  panels of Fig. 2 for more details). In other words, once the phase difference is decreased to a given critical value  $\varphi^* \approx \pi/3$  for the model parameters used in Fig. 2, Kondo correlations in the basis of the  $w$  fields are suppressed which translates into the  $d$  basis as a split central peak in the normal spectral function. Let us also stress out, that the phase-induced splitting of the central peak may be completely avoided in parameter regimes with very small hybridization  $\Gamma_S$  which is in complete analogy to SCIAM. The crucial point is to keep the value of  $\Gamma_S$  so small that for given interaction strength  $U$  the asymmetry parameter  $\delta$  is sufficiently small to avoid significant disruption of the Kondo peak.

Let us now follow the number and positions of all off-center peaks visible in the corresponding spectra of the  $\Delta \rightarrow \infty$  model with increasing the angle  $\varphi$  as seen in the basis of the  $d$  fields (the middle row of panels in Fig. 2

seen from left to right). At  $\varphi = 0$  (the first column), we see a pair of off-center peaks at  $\omega \approx \pm 2\Gamma_N$  and a second pair of highly suppressed peaks at  $\omega \approx \pm 12\Gamma_N$ . The two inner peaks have already been connected to the remnants of the Kondo resonance as seen in the basis of the  $w$  fields. The outer pair of peaks relates to the suppressed charge excitations of the underlying asymmetric SIAM in the basis of the  $w$  fields. Increasing the angle  $\varphi$  causes the  $\delta$  parameter of the underlying asymmetric SIAM to decrease. Consequently, the two inner peaks move towards each other until they finally merge together for  $\varphi^* \approx \pi/3$  to form the central Kondo-like peak discussed previously. The pair of originally suppressed peaks becomes on the other hand stronger and thus more noticeable since the corresponding charge excitations of the underlying asymmetric SIAM become stronger with decreasing  $\delta$ . Therefore, at around  $\varphi^*$ , when the Kondo-like central peak forms, two pairs of symmetrically placed off-center peaks become recognizable (at  $\varphi = 2\pi/3$  one notices two shoulders of the central peak). These two pairs move then towards  $\pm U/2$  which occurs at  $\varphi = \pi$ . Here, they correspond to the ordinary Hubbard peaks of the symmetric SIAM.

For the  $\Delta \rightarrow \infty$  model, we may thus encounter two distinctive spectral function shapes which cross over smoothly into each other. For  $\varphi < \varphi^*$  we observe one pair

of symmetrically positioned peaks that move towards the Fermi energy with increasing  $\varphi \rightarrow \varphi^*$  while the other pair of outer peaks is mostly unnoticeable. At  $\varphi \approx \varphi^*$  the inner peaks cross each other and continue to move towards  $\pm U/2$  with the increasing phase difference  $\varphi$ . The pair of the outer peaks becomes more pronounced at around  $\varphi^*$  where they also start to move noticeably towards the Fermi energy. At  $\varphi = \pi$ , they finally merge together with the inner pair of peaks at approximately  $\pm U/2$ . Taking together, the movement of the various peaks is highly reminiscent of the behavior of the ABS states of the SCIAM. For  $\varphi < \varphi^*$  the spectral function resembles the 0 phase while for  $\varphi > \varphi^*$  the behavior of the peaks shows analogy to the  $\pi$  phase of the SCIAM. Nevertheless, in both cases the presence of the normal lead causes the  $\Delta \rightarrow \infty$  model to acquire a singlet many-body ground state for all values of  $\varphi$  and no quantum phase transition is present in the three-terminal setup. We will thus refer to the  $\varphi < \varphi^*$  scenario as 0-like phase while for  $\varphi > \varphi^*$  the term  $\pi$ -like phase will be used. Moreover, for 0-like phase we have previously also discussed a second pair of peaks in the spectral function, which lies further the Fermi energy. Although, they can easily be interpreted within the effective asymmetric SIAM they cannot be explained as broadened analogs of ABS states of the SCIAM. Crucially, this outer pair of peaks appears because the corresponding many-body states can be excited due to the singlet nature of the ground state while in the SCIAM corresponding energy eigenstates do also exist, but they cannot be excited for  $\varphi < \varphi^*$ . Additional difference appears also in the  $\pi$ -like phase for  $\varphi > \varphi^*$ , where the presence of non-zero DOS around the Fermi energy due to the normal electrode always gives rise to the Kondo screening not present in the SCIAM at all. In the  $\pi$ -like phase we thus observe the coexistence of four broadened ABS states typical for the SCIAM with the Kondo resonance at the Fermi energy.

#### IV. FINITE-GAP MODEL

##### A. NRG calculations

As discussed in Sec. II C, the transformation  $\mathbb{T}$  maps the finite-gap three-terminal setup at the half-filling onto an NRG-tractable one-channel problem. In particular, in the basis of the  $w$  fields, the Hamiltonian describes an Anderson impurity coupled to a continuum of bath states with modified tunneling DOS which except of  $\varphi = \pi$  is particle-hole asymmetric. This can be shown by evaluating the hybridization function  $\Gamma^W(\omega)$  corresponding to  $\Sigma^W(\omega)$  as shown in the Appendix B. In the limit of infinitely wide band one obtains

$$\Gamma^W(\omega) = \frac{\Gamma_N}{2} + \frac{\Gamma_S |\omega| \Theta(\omega^2 - \Delta^2)}{\sqrt{\omega^2 - \Delta^2}} \left( 1 + \frac{\Delta}{\omega} \cos \frac{\varphi}{2} \right), \quad (43)$$

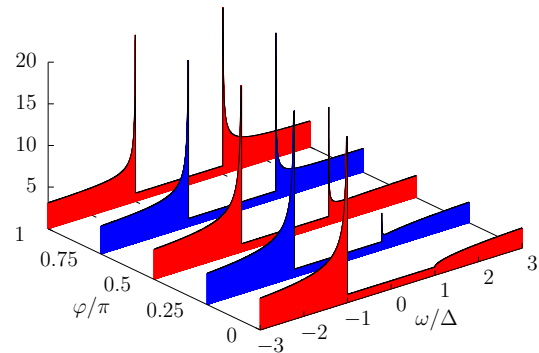


FIG. 3. Phase evolution of the tunneling DOS  $\Gamma^W(\omega)$  in the  $w$  basis for  $\Gamma_N/\Delta = 1$  and  $\Gamma_S/\Delta = 2$ . At  $\varphi = 0$ , only the left BCS singularity does appear and the resulting tunnelling DOS is highly asymmetric. Increasing  $\varphi$  diminishes the asymmetry while BCS singularities develop at both gap edges. The symmetry is fully restored only at  $\varphi = \pi$ .

where  $\Theta$  is the Heaviside step function. The phase evolution of hybridization function  $\Gamma^W(\omega)$  is shown in Fig. 3 for selected parameters. Note that only for  $\varphi = \pi$  the hybridization function is symmetric with asymmetry increasing towards  $\varphi = 0$ . Consequently, in the  $w$  basis, the particle-hole symmetry of the finite-gap three-terminal model is broken for  $\varphi \neq \pi$ . Moreover, asymmetry decreases with  $\varphi$  in analogy to the  $\Delta \rightarrow \infty$  case. Since  $\Gamma^W(\omega)$  is diagonal, the basis of the  $w$  fields allows us to employ the standard one-channel NRG method of Ref. [38]. To this end, we have utilized NRG Ljubljana code [40] in one-channel mode with leads given by the spin-unpolarized hybridization function  $\Gamma^W(\omega)$ . To suppress numerical oscillatory artefacts of NRG, we have used the intertwined  $z$ -discretization according to the scheme of Žitko et al. [45]. Explicitly,  $z = n/10$  with  $n \in \{0, \dots, 10\}$ . To achieve greater accuracy in the spectral function, the so-called self-energy trick has been also employed. The resulting spectral functions are then smoother and do also correctly reproduce discontinuities at the BCS gap edges which are otherwise smeared out. It is also important to stress that in the main body of the article we concentrate on the wide band with the half-bandwidth set to  $B/\Delta = 2000$ . The corrections required for the case of a narrow band are discussed separately in the Appendix B.

The experimentally accessible spectral functions in the  $d$  basis have been obtained by means of Eqs. (33) and (34) and the results are discussed in Sec. IV B. On-dot induced pairing  $\nu = \langle d_\downarrow d_\uparrow \rangle$  is trivially connected to the filling  $n_w$  in the basis of the  $w$  fields and can therefore be measured directly by the expectation value of the number operator as shown in Sec. IV C. On the contrary, the operator for the Josephson current requires both operators of the local  $d$  as well as the lead electrons. Thus, to evaluate the Josephson current we use the integral formula of Ref. [47] which involves the anomalous component of Green function in the  $d$  basis. The results on the on-dot induced

pairing and the Josephson current are also discussed in Sec. IV C.

Let us now briefly discuss the character of many-body spectrum for the present three-terminal setup with finite gap. Because of the normal metallic lead, the spectrum is expected to be continuous. Nevertheless, applying NRG means that the model is first discretized and mapped onto a semi-infinite Wilson chain. At each successive length of Wilson chain a low energy discrete spectrum is obtained while energies are typically rescaled by the logarithmic discretization factor  $\Lambda$ . In a fixed RG point, one observes a steady separation of energy levels which then comprise the energy spectrum of the corresponding universal Hamiltonian.

To disclose the level structure of the logarithmically discretized finite-gap three-terminal setup we have employed NRG Ljubljana by gradually increasing  $\varphi$  at the fixed model parameters while setting the length of the corresponding Wilson chain to reach the low temperature RG fixed point. The phase evolution of the resulting spectra is presented in Fig. 4. Although we have transformed the finite-gap three-terminal setup into the basis of the  $w$  fields, the transformation  $\mathbb{T}$  is unitary and the obtained spectra are thus independent of the use of the underlying basis of  $d$  or  $w$  fields. We also stress out that the parameter regime in Fig. 4 involves a sign reversal of the local pairing at  $\varphi_{\text{pair}}^* \approx 0.45\pi$  as well as the Josephson current reversal at  $\varphi_j^* \approx 0.5\pi$  (see the discussion in Sec. IV C).

At  $\varphi = \pi$ , the NRG energy spectrum consists of a singlet ground state, followed by the quadruplet of higher lying energy levels and an even higher lying sextet of energy levels. Such a discrete spectrum is typical for ordinary symmetric SIAM. When  $\varphi$  is decreased the quadruplet splits into two doublets and the sextet splits into a quadruplet with two additional singlets placed symmetrically around it. Such outcome corresponds, however, to the ordinary asymmetric SIAM. In other words, NRG establishes that the phase-dependent low energy many-body spectra of the logarithmically discretized finite-gap model are essentially indistinguishable from those for the ordinary particle-hole asymmetric SIAM at  $\varphi \neq \pi$  and the particle-hole symmetric SIAM at  $\varphi = \pi$ . The qualitative behavior of the spectral functions of the finite-gap three-terminal model is thus expected to essentially follow the results for the  $\Delta \rightarrow \infty$  case discussed in Sec. III, where the exact mapping onto the particle-hole asymmetric SIAM was shown explicitly. This way, NRG gives also an important insight into the physical consequences of the particle-hole asymmetry of the underlying model in the  $w$  basis which is completely given by its hybridization function  $\Gamma^W(\omega)$ . In other words, the universal Hamiltonian describing the low energy properties of the present model corresponds to the ordinary asymmetric SIAM for  $\varphi \neq \pi$  and goes smoothly over into the symmetric SIAM for  $\varphi \rightarrow \pi$ . Therefore, we may expect that the spectral properties of the finite-gap case are only quantitatively altered compared to the infinite-gap scenario.

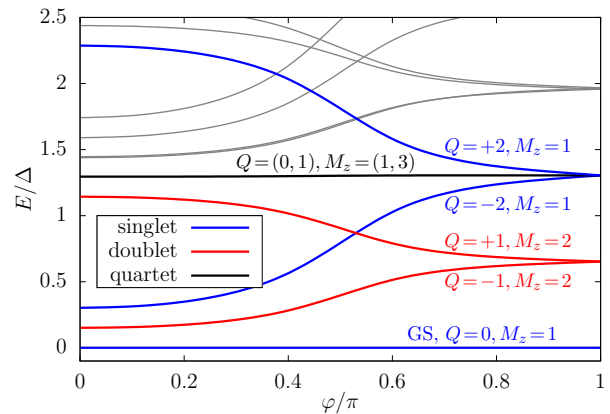


FIG. 4. Low energy eigenvalues of the logarithmically discretized Hamiltonian obtained using NRG Ljubljana for the half-bandwidth  $B/\Delta = 2000$ ,  $U/\Delta = 3$ ,  $\Gamma_S/\Delta = 1$  and  $\Gamma_N/\Delta = 0.01$ .  $Q$  is defined as the total charge of the Wilson chain measured with respect to the half-filling and  $M_z \equiv 1 + 2S_z$  with  $S_z$  being the overall magnetization of the Wilson chain.

Thus, quantitative changes in quantities like on-dot induced pairing and Josephson current are not related to the change of the ground state or the structure of the higher lying states, but to the fine details of the corresponding spectral functions as discussed in Secs. IV B and IV C.

## B. Spectral properties and the Kondo scale

The phase evolution of the normal spectral function in the basis of the  $d$  fields is shown in Fig. 5 for two values of  $U/\Delta$ . Let us first discuss the  $U/\Delta = 3$  case which incorporates features of 0-like as well as  $\pi$ -like phase as observed in the  $\Delta \rightarrow \infty$  case (panels (a) and (b) in Fig. 5). Since qualitatively finite-gap case does not differ much from the  $\Delta \rightarrow \infty$  case, we will only briefly sum up the most important points. At  $\varphi = 0$ , two broadened ABS-like peaks placed symmetrically around the Fermi energy are distinguishable. With increasing  $\varphi$ , both peaks move towards the Fermi energy and merge at a certain value  $\varphi^*$  which depends non-trivially on  $U$  and  $\Delta$ . Subsequently, for all  $\varphi > \varphi^*$  the central Kondo-like peak is present. Moreover, four side-peaks (corresponding to the two symmetrized Hubbard satellites in the  $w$  basis) also emerge. Increasing  $\varphi$  further shifts the two peaks on each side of the spectra together, until at  $\varphi = \pi$  they coalesce at approximately  $\pm U/2$ . At this point, the tunneling DOS is symmetric and the  $\varphi = \pi$  spectrum resembles the three-peak structure obtained for symmetric SIAM where two Hubbard satellites and one central Kondo peak are present. The second case with  $U/\Delta = 6$  is shown in panels (c) and (d) of Fig. 5. Here, the ratio  $\Gamma_S/\Delta$  is insufficient to generate particle-hole asymmetry leading to

the emergence of the 0-like phase. Such regimes are analogous to the observations made for SCIAM at sufficiently large values of  $U/\Delta$ .

To make the movement of the in-gap peaks explicitly manifest, we visualized the phase-dependent positions of their maxima via heatmaps as shown in Fig. 5b,d. We clearly observe in Fig. 5b their crossing at angle  $\varphi^*$ . When  $\varphi$  is further increased, the in-gap peaks move apart again. However, for all  $\varphi > \varphi^*$  two additional in-gap states emerge relatively close to the band edges. The two peaks for  $\varphi < \varphi^*$  can thus be related to the two ABS states of SCIAM in the 0 phase, while the four off-central peaks are in one-to-one correspondence with the four ABS states observed in the  $\pi$  phase of SCIAM. However, unlike in SCIAM the non-zero DOS around the Fermi energy gives rise also to the central Kondo-like resonance for all  $\varphi > \varphi^*$ . So in total, there are five in-gap peaks in the analog of  $\pi$  phase for the present model.

Taking together, the obtained spectra qualitatively correspond to the  $\Delta \rightarrow \infty$  model and the physical interpretation in terms of the particle-hole asymmetry of the underlying model in the basis of the  $w$  fields holds analogously. Nevertheless, there are quantitative differences to the  $\Delta \rightarrow \infty$  case which appear once integral quantities such as the filling  $n_w$  in the basis of the  $w$  fields are considered. For the  $\Delta \rightarrow \infty$  model, the filling  $n_w$  monotonically decreases from the  $n_w = 1$  value obtained at  $\varphi = \pi$  for all parameter regimes. In the finite-gap three-terminal case, there are parameter regimes where  $n_w$  first increases to values larger than 1 (positive effective chemical potential) and then starts to monotonically decrease to values smaller than 1 (negative effective chemical potential). Such integral properties are shown in Sec. IV C to be crucial for the system to exhibit effects such as pairing or Josephson current reversal which are typical of 0- $\pi$  transition observed in SCIAM. This means that the precise shape of spectral functions plays an important role when analyzing the finite-gap case.

Let us now move to the quantitative behavior in the 0-like phase. The pair of strongly pronounced in-gap peaks for  $\varphi < \varphi^*$  can easily be interpreted as the broadened ABS states of the purely superconducting case. To this end, it can be verified that their structure can be fitted well by Lorentzian line shapes centered around the frequency  $\omega_{\text{ABS}}$  of the broadened ABS maxima with  $\Gamma_N$  used as the broadening parameter. Consequently, for  $\varphi < \varphi^*$  the spectra may be not only qualitatively but also quantitatively interpreted as broadened ABS states of the pure SCIAM model. However, once  $\varphi$  approaches  $\varphi^*$  the broadening of the in-gap states becomes much larger and for  $\varphi > \varphi^*$  it does not match with  $\Gamma_N$ . On the other hand, the number of the in-gap peaks is still four and they correspond well to the ABS states of the  $\pi$  phase of the SCIAM.

On the other hand, in the  $\pi$ -like phase, one observes an unusual co-existence of the Kondo-like peak with four broadened ABS states ( $\varphi > \varphi^*$ ). Since the prerequisite of an effective Kondo screening is the non-zero tunnelling

DOS around the Fermi energy brought in by the normal electrode, the central peak forms for arbitrary values of  $U$  at  $\varphi = \pi$ . In Sec. IV A, we have already established the correspondence of the low energy many-body NRG spectra to that of the particle-hole asymmetric SIAM for  $\varphi < \pi$  with particle-hole asymmetry monotonically decreasing towards  $\varphi = \pi$  where it completely vanishes. In the basis of the  $w$  fields, one therefore observes that starting at the particle-hole symmetric case for  $\varphi = \pi$  and then decreasing  $\varphi$ , causes a gradual movement of the original Kondo peak away from the Fermi energy which is induced by the increasing particle-hole asymmetry. However, as long as  $\varphi > \varphi^*$  the increasingly large broadening does overcome this shift and symmetrization (33) still leads to a well defined central peak in the spectral function  $A_{\sigma N}^W(\omega)$ . Only when  $\varphi$  is decreased further, does the broadening of the central peak stop compensating for the rapid movement of the peak, so that the symmetrization (33) results in a doubly peaked spectral function  $A_{\sigma N}^W(\omega)$  in the basis of the  $w$  fields.

In the  $d$  basis, the lack or presence of a single central peak can be thus understood as a sign of the Kondo-like interaction-screening efficiency. To capture this quantitatively, we have extracted the phase-dependent Kondo temperature  $T_K$  as the half-width at half maximum (HWHM) value of the zero-energy peak in the spectra of the  $\pi$ -like phase. Comparison to  $T_K^N$ , when both superconducting leads are decoupled, is shown in Fig. 6. We observe that, in general,  $T_K$  is bigger in the hybrid case compared to the ordinary SIAM. However, this cannot be naively interpreted as the enhancement of the Kondo screening in the hybrid reservoirs since once we relate  $T_K^N$  not to just the decoupled BCS electrodes but to the three normal electrodes obtained by taking  $\Delta \rightarrow 0$  limit in the superconducting leads the  $T_K$  would be smaller. However, approaching  $\varphi^*$  from the  $\pi$ -like phase clearly enhances  $T_K$  as shown in Fig. 6. Moreover, as hypothesized already in Ref. [32],  $T_K$  is proportional to  $\cos^2(\varphi/2)$  with only very small deviations appearing when approaching  $\varphi \rightarrow \varphi^*$ . In the 0-like phase the central Kondo-like peak vanishes and the definition of  $T_K$  as HWHM of the corresponding peak becomes meaningless.

### C. Pairing and Josephson current

Let us now address also the transport properties in the hybrid three-terminal structure. Since they have been already obtained in Ref. [32] using QMC, we will review the NRG results only briefly and concentrate mostly on how transport properties may be extracted from the transformed basis of the  $w$  fields. Although the  $w$  basis allows to obtain a simpler Hamiltonian, it requires redefinition of the reservoir and thus also the geometry of the setup. The transport properties are however measured in the original  $d$  basis. In particular, superconducting effects are connected to the off-diagonal terms in the Hamiltonian expressed in the  $d$  basis which are then rotated

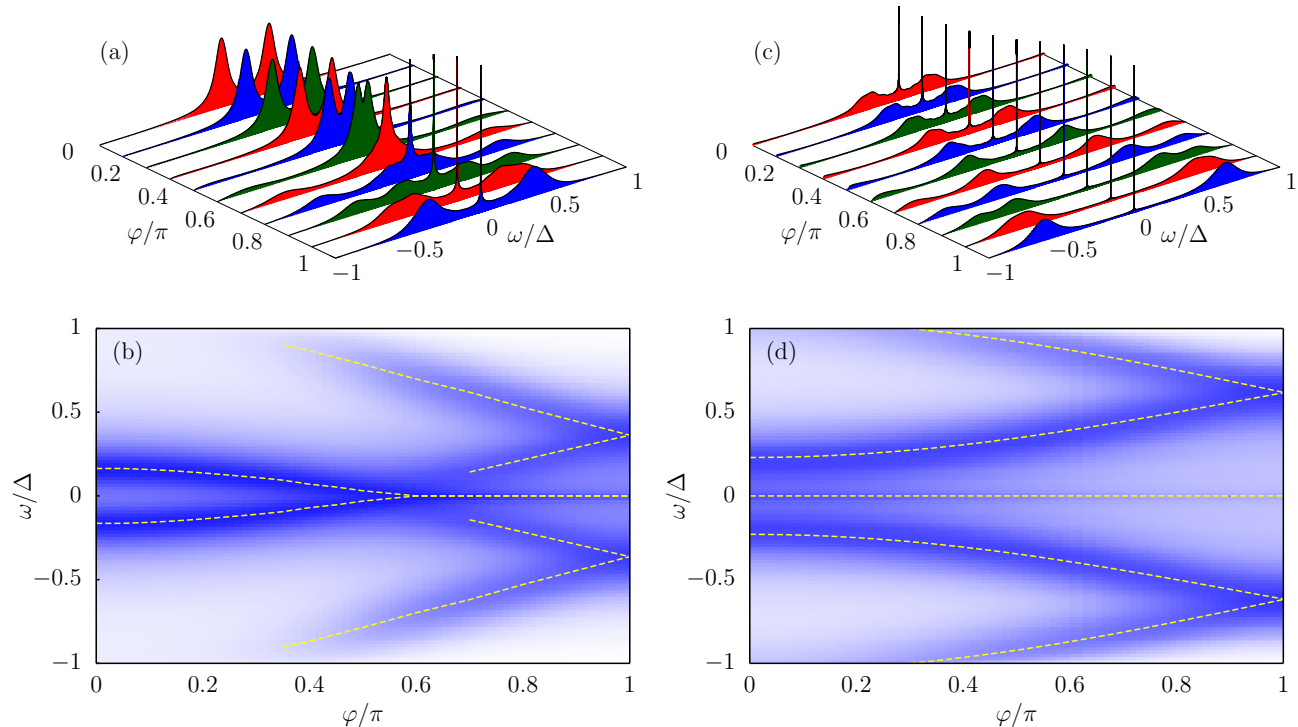


FIG. 5. (a) Phase evolution of the spectral function  $A_N^D(\omega)$  in the sub-gap region of the finite-gap three-terminal setup for  $U/\Delta = 3$ ,  $\Gamma_N/\Delta = 0.1$ ,  $\Gamma_S/\Delta = 1$  and half-bandwidth  $B/\Delta = 2000$ . For  $\varphi < \varphi^* \approx 0.55\pi$  one observes a pair of broadened ABS states while for  $\varphi > \varphi^*$  an additional pair of broadened ABS states and an additional central Kondo-like peak do appear. In an analogy to the SCIAM, for  $\varphi < \varphi^*$  the regime is referred to as the 0-like phase while for  $\varphi > \varphi^*$  as the  $\pi$ -like phase. (b) Heatmap corresponding to panel (a) highlights the phase-dependent position of the maxima of the in-gap peaks (dashed lines). (c) Phase evolution of the spectral function  $A_N^D(\omega)$  for the finite-gap three-terminal setup. All parameters apart from  $U/\Delta = 6$  are the same as in panel (a). The Kondo correlations dominate the system which remains in the  $\pi$ -like phase for all values of  $\varphi$ . For sufficiently large  $U$ , such a scenario does occur also in the SCIAM. (d) Heatmap corresponding to panel (c) shows the phase-dependent position of the maxima of the in-gap peaks (dashed lines).

to the diagonal elements of the Green function in the  $w$  basis. All effects related to the off-diagonal Green functions are therefore to be extracted by suitable backwards transformations. Let us first discuss the on-dot induced pairing  $\nu$  which is indirectly related to the Josephson current. While the on-dot induced pairing  $n_w$  in the  $w$  basis is by definition zero as  $G^W(\omega)$  has no off-diagonal entries, it turns out that the filling  $n_w$  in  $w$  basis is directly related to the pairing observed in the original basis as follows from simple application of the transformation  $\mathbb{T}$  to the definition of  $\nu$ . In particular

$$\nu \equiv \langle d_\downarrow d_\uparrow \rangle = \frac{1}{2} - \frac{n_w}{2}. \quad (44)$$

The above equation connects the change of the filling in the basis of the  $w$  fields from  $n_w < 1$  to  $n_w > 1$  with switching sign of the on-dot induced pairing  $\nu$  in the basis of the  $d$  fields from positive to negative values. In the case of  $\Delta \rightarrow \infty$  model the mapping onto the asymmetric SCIAM fixed the possible values of filling to  $n_w < 1$  which

effectively prohibited any sign reversal of the on-dot induced pairing. In the case of the finite-gap three-terminal setup, one can show that both fillings larger as well as smaller than 1 are possible. The on-dot induced pairing for several values of  $\Gamma_N/\Gamma_S$  is shown in Fig. 7. The observed dependencies are in a close relation to the well-known result obtained for SCIAM. However, there is no jump in the on-dot induced pairing that would indicate a true phase transition. Instead, the on-dot induced pairings for all parameter regimes are continuous functions and a crossover region of significant drop is only visible for small values of  $\Gamma_N/\Gamma_S$ . For small enough hybridization  $\Gamma_N$ , see the phase dependencies for  $\Gamma_N/\Gamma_S = 0.01$  and  $\Gamma_N/\Gamma_S = 0.1$  in Fig. 7, the drop may even lead to sign reversal of pairing at  $\varphi_{\text{pair}}^*$ . Such pairing reversal is however not directly related to the change of spectral properties at  $\varphi^*$  and the two values are generally different, i. e.  $\varphi^* \neq \varphi_{\text{pair}}^*$ . Nevertheless, for  $\Gamma_N \rightarrow 0$  the value of  $\varphi_{\text{pair}}^*$  approaches  $\varphi^*$ . The comparison of the present results to QMC is shown in the the Appendix C, where

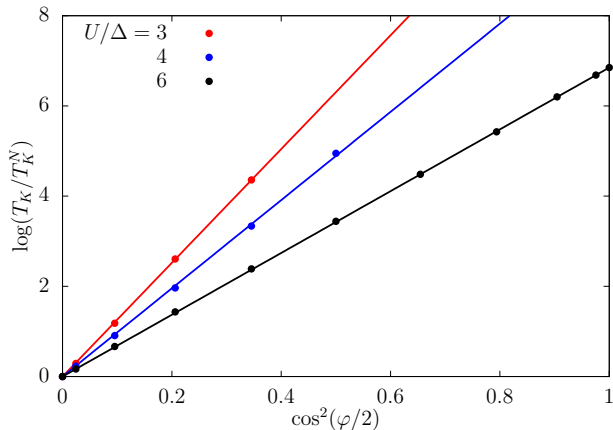


FIG. 6. Phase dependence of the Kondo temperature  $T_K$  obtained by NRG for the half-bandwidth  $B/\Delta = 2000$ ,  $U/\Delta = 3$ ,  $\Gamma_N/\Delta = 0.1$ ,  $\Gamma_S/\Delta = 1$ . The Kondo temperature is determined as the half-width at half maximum value of the central Kondo-like peak observed in the  $\pi$ -like phase.

also the effect of the finite bandwidth on the phase dependency in the crossover region is discussed in detail. At this place, it is sufficient to note that deep in the 0-like or  $\pi$ -like phase QMC and NRG agree well within their numerical accuracy.

While the spectra as well as the on-dot induced pairing could be directly transformed back into the  $d$  basis, the operator for the Josephson current  $J$  involves also the lead  $c$  electrons and we have to resort to an expression involving the anomalous component of the Green function [47]

$$\frac{J}{2\Delta} = \sin \frac{\varphi}{2} \int_{-\infty}^{+\infty} \frac{d\omega}{\pi} f(\omega) \text{Im} [G_A^D(\omega) \Sigma_A^D(\omega)], \quad (45)$$

where  $f(\omega)$  is the Fermi-Dirac distribution,  $G_A^D$  is the anomalous Green function in the  $d$  basis and  $\Sigma_A^D(\omega)$  (26) in the limit of the infinite bandwidth reads

$$\begin{aligned} \Sigma_A^D(\omega) &= \frac{\Gamma_S}{\sqrt{\Delta^2 - \omega^2}} \Theta(\Delta^2 - \omega^2) \\ &+ \frac{i\Gamma_S \text{sgn}(\omega)}{\sqrt{\omega^2 - \Delta^2}} \Theta(\omega^2 - \Delta^2). \end{aligned} \quad (46)$$

The integral (45) involving anomalous components of the Green function requires high frequency resolution and reliable broadening procedure when applying NRG.

The results of phase-dependent Josephson current are shown in Fig. 7 for  $U/\Delta = 3$  at different ratios of  $\Gamma_N/\Gamma_S$ . The sign reversal of the Josephson current occurs only for small hybridization strengths  $\Gamma_N$  which clearly shows that Kondo correlations are important in the system and may overcome the superconducting correlations. Once again, the  $\varphi_j^*$  at which sign reversal occurs does not match  $\varphi^*$  from crossing of the ABS states nor  $\varphi_{\text{pair}}^*$ , but all three values tend to be the same for  $\Gamma_N \rightarrow 0$ .

## V. CONCLUSIONS

We have investigated a general finite-gap model of QD with an arbitrary Coulomb repulsion attached to the hybrid reservoir composed of one normal lead and two BCS leads with an arbitrary phase difference. To obtain reliable and method-unbiased results on phase-dependent spectral functions of the problem, the standard NRG was employed. However, the full problem with three types of leads requires within the standard NRG approach to implement three-channel calculations which poses several non-trivial challenges [41]. To circumvent the numerical limitations we have thus introduced a unitary transformation  $\mathbb{T}$  of the local dot electrons  $d$ , which allows to reformulate the finite-gap model with hybrid phase-biased reservoirs at the half-filling, despite the general belief [38], as a one channel problem. Moreover, the approach is by no means limited to the non-zero values of  $\Gamma_N$  and holds also in the case of the decoupled normal electrode where the three-terminal setup goes over into the ordinary SCIAM. Consequently, at the half-filling the transformation  $\mathbb{T}$  transforms SCIAM onto the SIAM with the tunneling DOS that incorporates a hard gap. The vanishing tunnelling DOS around the Fermi energy consequently hampers the formation of the Kondo resonance. However, the quantitative understanding requires to apply NRG techniques with either finite-sized Wilson chains, when the standard logarithmic discretization around the Fermi energy is used, or to modify the discretization to avoid the energy range of the hard gap.

In this regard, the present three-terminal reservoir has always a non-zero tunneling DOS around the Fermi energy and a standard logarithmic discretization in the transformed basis of the fields  $w_\sigma$  with  $\sigma \in \{\uparrow, \downarrow\}$  can be employed. Thus, the open-source NRG Ljubljana code could be employed unaltered. The obtained phase-dependent spectral functions showed behavior similar to that observed in the 0 and  $\pi$  phases of the SCIAM. Thus, two regimes, referred here as the 0-like and the  $\pi$ -like phase, have been identified, see Figs. 5 and 7 for more details. However, the two regimes do not constitute separate phases, because even though the normal electrode may be only weakly hybridized with the remaining system, it always provides a non-zero tunnelling DOS around the Fermi energy which enables the formation of the Kondo many-body ground state of the singlet nature. In other words, 0-like and the  $\pi$ -like phases represent separate regimes which are smoothly interconnected with each other when the phase bias  $\varphi$  is changed continuously. The width of the resulting crossover region, as shown in Figs. 5 and 7, is roughly proportional to the hybridization  $\Gamma_N$ .

In more detail, when the hybridization  $\Gamma_N$  is sufficiently small, see Fig. 5, one obtains quite a narrow crossover region in which the off-center in-gap peaks of the corresponding spectral function do cross at  $\varphi^*$ . Moreover, one also observes sign changes in the transport properties in the crossover region with the on-dot induced

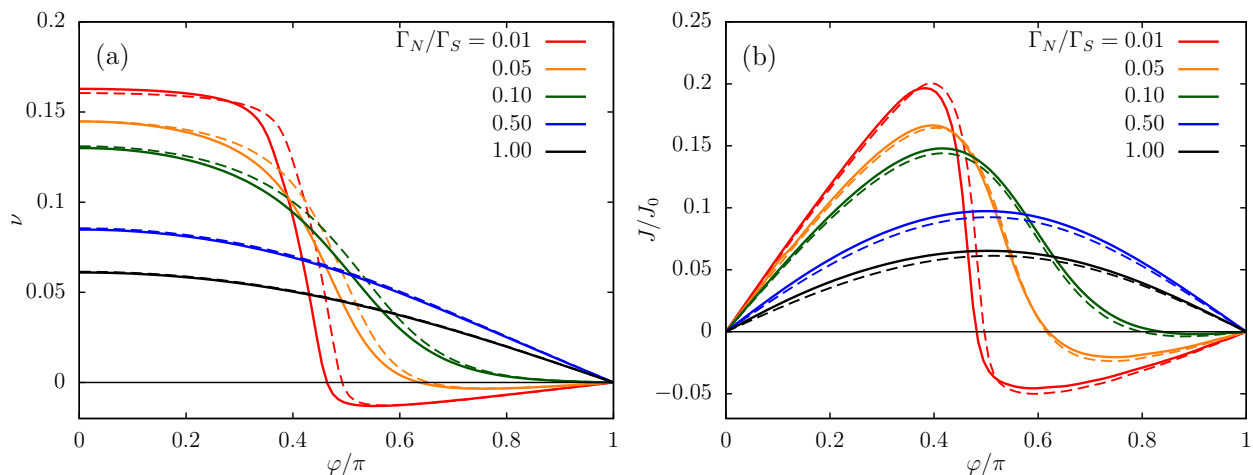


FIG. 7. (a) Phase evolution of the on-dot induced pairing  $\nu \equiv \langle d_{\downarrow} d_{\uparrow} \rangle$  of the finite-gap three-terminal setup at  $T = 0$  obtained using NRG Ljubljana in the basis of the  $w$  fields with subsequent use of Eq. (44) for the half-bandwidth  $B/\Delta = 2000$  (solid lines) and  $B/\Delta = 100$  (dashed lines). Parameters of the model are  $U/\Delta = 3$  and  $\Gamma_S/\Delta = 1$  while  $\Gamma_N$  varies. (b) Phase evolution of the Josephson current  $J$  obtained using NRG Ljubljana in the basis of the  $w$  fields with subsequent use of Eq. (45) for the same parameters as in panel (a).

pairing changing sign at  $\varphi_{\text{pair}}^*$  and the Josephson current at  $\varphi_j^*$ , see Fig. 7 for more details. Although generally the values of  $\varphi^*$ ,  $\varphi_{\text{pair}}^*$  and  $\varphi_j^*$  do not equal, they do so in the limit of  $\Gamma_N \rightarrow 0$ , where they reach the SCIAM value of the critical phase bias of the  $0-\pi$  transition. Moreover, at large values of  $\Gamma_N$  pairing and Josephson current are always positive,  $\varphi_{\text{pair}}^*$  and  $\varphi_j^*$  are thus not even defined while the distinct spectral properties of the  $0$ -like and the  $\pi$ -like phase are still present. The identification of the  $0$ -like and the  $\pi$ -like phases is therefore always based only on their spectral properties. For  $\varphi > \varphi^*$  the defining spectral property of the  $\pi$ -like phase is the presence of the two pairs of the in-gap peaks which merge together at  $\varphi = \pi$  and the presence of a central Kondo-like resonance. The two pairs of the in-gap peaks show an analogous phase-dependent behavior as the ABS states of the SCIAM (see the heatmaps in Fig. 5). The two pairs of the in-gap peaks can therefore be understood as broadened analogs of the ABS states of the SCIAM. However, unlike in the SCIAM, the tunneling DOS due to the presence of the normal lead is non-zero around the Fermi energy which causes an effective screening of the spin of the QD in the  $\pi$ -like phase as manifested by the presence the Kondo resonance in the spectral function. Thus, unlike in the SCIAM, in the finite-gap three-terminal setup the broadened ABS states do co-exist with the Kondo resonance in the  $\pi$ -like phase, see panels (a) and (c) in Fig. 5 for more details. Nevertheless, at  $\varphi^*$  the central peak at the Fermi energy splits and can no longer be attributed to Kondo-like correlations since the effective underlying model is already far from the half-filling so that charge excitations dominate. For  $\varphi < \varphi^*$  the spectral weight at the Fermi energy tends to zero with further decreasing the phase difference  $\varphi$ , a region corresponding to the  $0$ -like phase. Here, the split peak can be

interpreted in terms of two broadened ABS states with their phase-dependent behavior resembling the SCIAM. However, such a  $0$ -like phase has an additional pair of low-intensity peaks at higher frequencies, which (unlike in SCIAM) can be excited in the one-particle manner due to admixtures of the doublet state induced by the coupling to the normal lead.

Such complex behavior is qualitatively explained via the transformation  $\mathbb{T}$  which is thus not merely a technical tool for the implementation of NRG. The transformation  $\mathbb{T}$  maps the Hamiltonian of the three-terminal model at the half-filling onto the SIAM with a structured tunneling DOS shown in Fig. 3. The tunneling DOS in the basis of the  $w$  fields is at  $\varphi = 0$  highly particle-hole asymmetric. The asymmetry is then continuously diminished with increasing  $\varphi$  and vanishes completely at  $\varphi = \pi$ . As shown in Fig. 4 the particle-hole asymmetry of the tunneling DOS effectively acts as the particle-hole asymmetry in an ordinary SIAM with the concomitant increase of the Kondo temperature upon increasing the asymmetry followed by entering the mixed valence regime and eventually complete destruction of the Kondo resonance. The Kondo temperature  $T_K$  can be quantitatively assessed via the phase-dependent HWHM of the central Kondo-like peak. The analysis in Sec. IV C (see also Fig. 6) showed that  $\log T_K$  follows (almost up to the value of  $\varphi^*$ ) the  $\cos^2(\varphi/2)$  trend hypothesized already in Ref. [32] based on the infinite-gap limit of the present model and the second-order perturbation theory.

Moreover, using the transformation  $\mathbb{T}$  we have also obtained the phase-dependent on-dot induced pairing and the phase-dependent Josephson current in various parametric ranges. Results in the limit of the infinitely wide band are presented in Fig. 7, where also effects of finite width of the band are shown (with a detailed deriva-

tion given in the Appendix B). Incorporating these corrections allowed also for comparison with another numerically exact method, the continuous-time hybridization expansion (CT-HYB) QMC, which demonstrates an agreement between both methods in the regions outside of the crossover while the crossover itself shows large temperature dependence, see Appendix C. As already discussed, the resulting pairing and supercurrent reversals do not occur exactly at  $\varphi^*$  identified from the spectral functions. Moreover, sign reversals appear only at sufficiently low ratios  $\Gamma_N/\Gamma_S$ . Once a given threshold is exceeded the Kondo screening dominates the system, superconducting correlations are essentially suppressed and only modify the phase-dependent transport. This behavior is always enhanced by increasing the interaction strength, reducing the gap size, or increasing the hybridization of the normal lead. The observation of the  $0-\pi$ -like crossover is thus possible only in a fairly small part of the parameter space corresponding to the weak coupling of the normal lead to the QD.

The mapping  $\mathbb{T}$  not only significantly reduces the complexity of the hybrid normal-superconductor reservoirs during the NRG implementation, but it also allows for conceptual understanding of the competing Kondo and Josephson effects via the particle-hole asymmetric SIAM. In this regard, it is worth mentioning that the transformation  $\mathbb{T}$  applies in the same form also to the SCIAM, i.e., an interacting quantum dot coupled to two superconducting leads with hard gap in the spectrum, leading to its mapping onto the problem of normal Anderson impurity coupled to an insulator-like electronic reservoir with a hard spectral gap around the Fermi level. The original  $2 \times 2$  matrix formulation goes then over into a scalar one. This simplification may even allow for new analytical insights and is thus worth further pursuits. Moreover, the limitation to strict half-filling is not as stringent as it might seem since as shown in Ref. [48, Fig. 3b] in the most interesting Kondo regime of the SCIAM model, the results are in fact independent of the value of the particle-hole asymmetry for quite a wide range of its value. Therefore, the results obtained for the particle-hole symmetric model should be applicable also rather far away from the half-filling regime which makes the transformed scalar version of the SCIAM model practically relevant.

## ACKNOWLEDGMENTS

We acknowledge discussions with Rok Žitko, Martin Žonda, and Václav Janiš. This work was supported by Grant No. 19-13525S of the Czech Science Foundation (PZ, TN), by grant INTER-COST LTC19045 (VP), by the COST Action NANOCOHYBRI (CA16218) (TN), the National Science Centre (NCN, Poland) via Grant No. UMO-2017/27/B/ST3/01911 (TN) and by The Ministry of Education, Youth and Sports from the Large Infrastructures for Research, Experimental Development and Innovations project “IT4Innovations National Super-

computing Center LM2015070” (VP). Access to computing and storage facilities owned by parties and projects contributing to the National Grid Infrastructure Meta-Centrum provided under the programme “Projects of Large Research, Development, and Innovations Infrastructures” (CESNET LM2015042) is also appreciated.

## Appendix A: Interaction term in the basis of the $w$ fields

To calculate the interaction part  $H_U$  in the basis of the  $w$  fields, let us first apply the transformation  $\mathbb{T}_1^-$  to the following quantities

$$d_{\uparrow}^{\dagger}d_{\uparrow} = \frac{1 + w_{\uparrow}^{\dagger}w_{\uparrow} - w_{\downarrow}^{\dagger}w_{\downarrow}}{2} - \frac{w_{\uparrow}^{\dagger}w_{\downarrow}^{\dagger} + w_{\downarrow}w_{\uparrow}}{2}, \quad (\text{A1})$$

$$d_{\downarrow}^{\dagger}d_{\downarrow} = \frac{1 - w_{\uparrow}^{\dagger}w_{\uparrow} + w_{\downarrow}^{\dagger}w_{\downarrow}}{2} - \frac{w_{\uparrow}^{\dagger}w_{\downarrow}^{\dagger} + w_{\downarrow}w_{\uparrow}}{2}. \quad (\text{A2})$$

We also define  $\mu = w_{\uparrow}^{\dagger}w_{\uparrow} - w_{\downarrow}^{\dagger}w_{\downarrow}$  and  $\xi = w_{\uparrow}^{\dagger}w_{\downarrow}^{\dagger} + w_{\downarrow}w_{\uparrow}$  which satisfy

$$1 - \mu^2 = \xi^2 = -w_{\uparrow}^{\dagger}w_{\uparrow} + 2n_{w\uparrow}n_{w\downarrow} + w_{\downarrow}w_{\downarrow}^{\dagger}, \quad (\text{A3})$$

$$\mu\xi = \xi\mu = 0, \quad (\text{A4})$$

where  $n_{w\uparrow} = w_{\uparrow}^{\dagger}w_{\uparrow}$  and  $n_{w\downarrow} = w_{\downarrow}^{\dagger}w_{\downarrow}$ . Using these relations we obtain

$$\begin{aligned} d_{\uparrow}^{\dagger}d_{\uparrow}d_{\downarrow}^{\dagger}d_{\downarrow} &= \frac{1 - \mu^2 - \mu\xi + \xi\mu - 2\xi + \xi^2}{4} \\ &= n_{w\uparrow}n_{w\downarrow} - \frac{1}{2}W^{\dagger}(\sigma_x + \sigma_z)W. \end{aligned} \quad (\text{A5})$$

Consequently, applying the  $\mathbb{T}_1^-$  transformation to the interaction term  $H_U$  gives

$$\begin{aligned} H_U &= U d_{\uparrow}^{\dagger}d_{\uparrow}d_{\downarrow}^{\dagger}d_{\downarrow} - \frac{U}{2}D^{\dagger}(\sigma_x + \sigma_z)D \\ &= U w_{\uparrow}^{\dagger}w_{\uparrow}w_{\downarrow}^{\dagger}w_{\downarrow}, \end{aligned} \quad (\text{A6})$$

which in the basis of the  $w$  fields obtains the form of the ordinary Hubbard term. Notice that the additional quadratic term in  $H_U$  in the basis of the  $d$  fields cancels exactly the quadratic term of Eq. (A5) when correspondingly transformed.

## Appendix B: Corrections due to the finite bandwidth

It is now our aim to give a detailed derivation of the self-energy contribution  $\Sigma^D$  for the hybrid three-terminal setup under the study. The discussion simplifies when  $\Sigma^D$  is divided right from the beginning into its contribution  $\Sigma_N^D$  due to just the normal lead and its superconducting contribution  $\Sigma_S^D$  due to the two phase-biased superconducting leads. Explicitly:

$$\Sigma^D(z) = \Sigma_N^D(z) + \Sigma_S^D(z) \quad (\text{B1})$$

with

$$\begin{aligned}\Sigma_N^D(z) &= \sum_{\mathbf{k}} \mathbb{V}_{N\mathbf{k}} (z + \mathbb{1} - \mathbb{E}_{N\mathbf{k}})^{-1} \mathbb{V}_{N\mathbf{k}} \\ \Sigma_S^D(z) &= \sum_{\alpha \in \{L,R\}, \mathbf{k}} \mathbb{V}_{\alpha\mathbf{k}} (z + \mathbb{1} - \mathbb{E}_{\alpha\mathbf{k}})^{-1} \mathbb{V}_{\alpha\mathbf{k}}\end{aligned}\quad (\text{B2})$$

with  $z$  being an arbitrary complex number. Later, only the functional form only infinitesimally close to the real axis needs to be resolved. For that we set  $z = \omega^+ \equiv \omega + i\eta$  with  $\omega$  being a real frequency and  $\eta$  being an infinitesimally small positive number, thus taking the cut slightly above the real axis. The self-energy contribution from the normal lead for the constant density of states in the band  $\rho_0$  is well-known and reads as

$$\Sigma_N^D(\omega^+) = i\Gamma_N \mathbb{1} \quad (\text{B3})$$

with  $\Gamma_N \equiv \pi\rho_0|V_N|^2$ . The superconducting part on the other hand is non-trivial and shall be treated here in more detail. It is defined as

$$\Sigma_S^D(\omega^+) = \sum_{\alpha \in \{L,R\}, \mathbf{k}} \mathbb{V}_{\alpha\mathbf{k}} (\omega^+ \mathbb{1} - \mathbb{E}_{\alpha\mathbf{k}})^{-1} \mathbb{V}_{\alpha\mathbf{k}} \quad (\text{B4})$$

with notation following that of the main article. The inverse matrix (the resolvent) appearing in Eq. (B4) yields

$$(\omega^+ \mathbb{1} - \mathbb{E}_{\alpha\mathbf{k}})^{-1} = \frac{\omega^+ \mathbb{1} + \Delta_\alpha C_\alpha \sigma_x - \Delta_\alpha S_\alpha \sigma_y + \varepsilon_{\mathbf{k}} \sigma_z}{(\omega + i\eta)^2 - \Delta^2 - \varepsilon_{\mathbf{k}}^2}. \quad (\text{B5})$$

Since  $\eta$  is infinitesimally small the denominator can be simplified to

$$(\omega^+ \mathbb{1} - \mathbb{E}_{\alpha\mathbf{k}})^{-1} = \frac{\omega \mathbb{1} + \Delta_\alpha C_\alpha \sigma_x - \Delta_\alpha S_\alpha \sigma_y + \varepsilon_{\mathbf{k}} \sigma_z}{\omega^2 - \Delta^2 - \varepsilon_{\mathbf{k}}^2 + i\eta \text{sgn}(\omega)}. \quad (\text{B6})$$

Considering now  $\mathbb{V}_{\alpha\mathbf{k}} \equiv V_S \mathbb{1}$  with  $V_S$  being real, we may use the resolvent expression (B6) and simplify Eq. (B4) to obtain  $\Sigma_S^D(\omega^+)$  as

$$\Sigma_S^D(\omega^+) = 2|V_S|^2 \sum_{\mathbf{k}} \frac{\omega \mathbb{1} - \Delta \cos\left(\frac{\varphi}{2}\right) \sigma_x + \varepsilon_{\mathbf{k}} \sigma_z}{\omega^2 - \Delta^2 - \varepsilon_{\mathbf{k}}^2 + i\eta \text{sgn}(\omega)}. \quad (\text{B7})$$

Moreover, assuming a constant density of states  $\rho_0$  in the band the  $\mathbf{k}$  summations may be replaced by the energy integration:

$$\Sigma_S^D(\omega^+) = 2\Gamma_S \left[ \omega \mathbb{1} - \Delta \cos\left(\frac{\varphi}{2}\right) \sigma_x \right] F(\omega^+), \quad (\text{B8})$$

where  $\Gamma_S \equiv \pi\rho_0 V_S$  and

$$F(\omega^+) = \frac{1}{\pi} \int_{-B}^B \frac{d\varepsilon}{\omega^2 - \Delta^2 - \varepsilon^2 + i\eta \text{sgn}(\omega)} \quad (\text{B9})$$

with  $B$  being the half-bandwidth and the term proportional to  $\sigma_z$  vanished due to the integrand being an odd

function of  $\varepsilon$ . To resolve the integrals we need to distinguish the in-gap region  $\Delta^2 - \omega^2 > 0$  where the integration is trivial (the  $\eta \rightarrow 0$  limit can be taken directly) with

$$F(\omega^+) = -\frac{2}{\pi\sqrt{\Delta^2 - \omega^2}} \arctan\left(\frac{B}{\sqrt{\Delta^2 - \omega^2}}\right). \quad (\text{B10})$$

The out-of-the-gap region  $\omega^2 - \Delta^2 > 0$  has poles in the complex plane which need to be carefully taken into account by employing the Sokhotski-Plemelj theorem to obtain

$$F(\omega^+) = -\frac{i \text{sgn}(\omega)}{\sqrt{\omega^2 - \Delta^2}} + \frac{\ln\left(\frac{B + \sqrt{\omega^2 - \Delta^2}}{B - \sqrt{\omega^2 - \Delta^2}}\right)}{\pi\sqrt{\omega^2 - \Delta^2}}. \quad (\text{B11})$$

The resulting  $\Sigma^D(\omega^+)$  has thus a non-zero imaginary part only outside of the in-gap region while all effects of the finite-sized band are to be found in its real part which is non-zero in the whole band. However, once the limit  $B \rightarrow \infty$  is taken the real part out of the in-gap region vanishes also.

Taking together, the self-energy contribution  $\Sigma^D(\omega^+)$  takes the form of (26), where

$$\Sigma_N^D(\omega) = i\Gamma_N + 2\Gamma_S F(\omega^+) \quad (\text{B12})$$

and

$$\Sigma_A^D(\omega) = -2\Gamma_S \Delta \cos\left(\frac{\varphi}{2}\right) F(\omega^+). \quad (\text{B13})$$

### Appendix C: Comparison of the NRG results with QMC

In order to assess the ability of the presented NRG scheme to provide reliable results on the integral quantities like the on-dot induced pairing and the Josephson current, we compare the results with a numerically exact continuous-time, hybridization-expansion (CT-HYB) QMC, as this method was already successfully used to study both the two-terminal [48] and three-terminal [32] setups and agrees with standard NRG results well within the QMC error bars.

The CT-HYB calculation is performed in the original basis of  $d$  fields employing off-diagonal elements of the hybridization function using the TRIQS/CTHYB solver [49]. The total Hamiltonian of the system does not conserve particle number, therefore the superconducting pairing is introduced to the method using a canonical particle-hole transformation in the spin-down sector, mapping the system to an impurity Anderson model with attractive interaction [50, 51]. As CT-HYB is an inherently finite-temperature method, all calculations were performed at  $k_B T / \Delta = 0.025$ . All results are calculated for half-bandwidth  $B = 100\Delta$  and a cutoff in Matsubara frequencies  $\omega_n^{max} \approx 314\Delta$ .

The comparison of the results of the presented NRG scheme with CT-HYB is plotted in Fig 8. NRG results

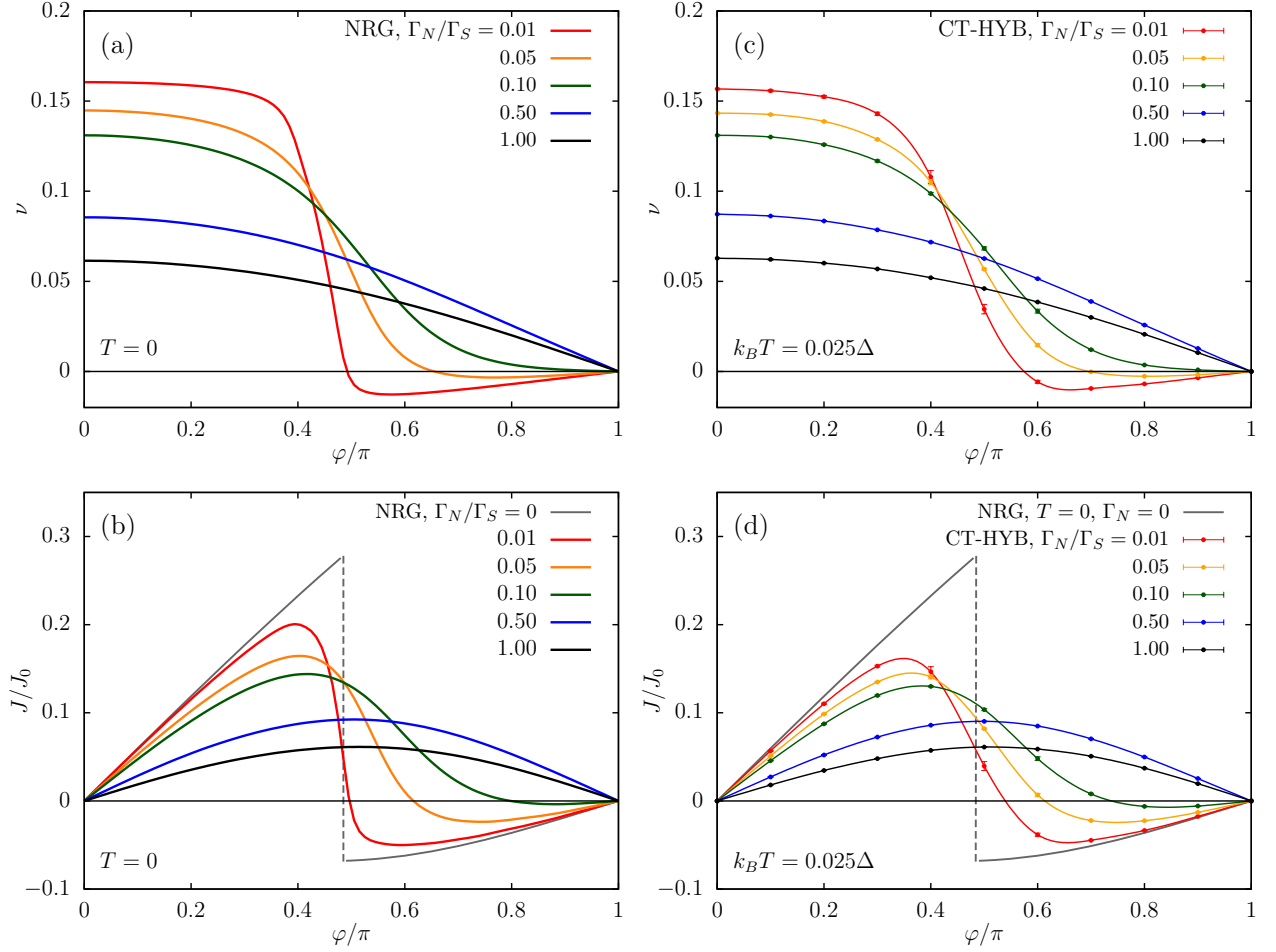


FIG. 8. Left column: Phase-dependent on-dot pairing  $\nu \equiv \langle d_{\downarrow} d_{\uparrow} \rangle$  (panel a) and the Josephson current  $J$  (panel b) calculated using NRG at zero temperature in the basis of the  $w$  fields with subsequent use of Eqs. (44) and (45) for the parameters  $B/\Delta = 100$ ,  $U/\Delta = 3$ ,  $\Gamma_S/\Delta = 1$  and various values of  $\Gamma_N$ . Right column: Equivalent results calculated using CT-HYB QMC in the basis of the  $d$  fields for small finite temperature  $k_B T/\Delta = 0.025$  (symbols with error bars): on-dot pairing  $\nu$  (panel c) and Josephson current  $J$  (panel d) with  $J_0 = 2e\Delta/\hbar$ . Lines are splines of QMC data and serve only as a guide to the eye.

for the induced pairing  $\nu$  as a function of phase difference  $\varphi$  for  $B/\Delta = 100$ ,  $U/\Delta = 3$ ,  $\Gamma_S = \Delta$  and various values of  $\Gamma_N$  at zero temperature are plotted in panel a (top left). The importance of the finite-bandwidth corrections were already discussed in Fig. 7. The equivalent results of CT-HYB for small finite temperature are plotted in panel c (top right). The curves match within QMC error bars for small and large values of  $\varphi$ . In the crossover region, the results slightly differ as the finite temperature is a source of additional smearing, having a similar effect as  $\Gamma_N$ , as already discussed in Ref. [32]. In panel b (bot-

tom left) we plotted the NRG results for the Josephson current for the same set of parameters as in panel a. We added a  $\Gamma_N = 0$  result from Ref. [32] to mark the position of the QPT in a case of detached normal electrode. The relevant CT-HYB result is again plotted in panel d (bottom right). Comparison again shows good agreement up to the finite-temperature effects, proving that the presented NRG scheme is able to provide correct results on the Josephson current even though it cannot be measured directly and must be reconstructed from the calculated anomalous spectral function.

- [1] S. J. Tans, M. H. Devoret, H. Dai, A. Thess, R. E. Smalley, L. J. Geerligs, and C. Dekker, *Nature* **386**, 474 (1997).  
 [2] A. Y. Kasumov, R. Deblock, M. Kociak, B. Reulet, H. Bouchiat, I. I. Khodos, Y. B. Gorbatov, V. T. Volkov,

- C. Journet, and M. Burghard, *Science* **284**, 1508 (1999).  
 [3] P. Jarillo-Herrero, J. A. van Dam, and L. P. Kouwenhoven, *Nature* **439**, 953 (2006).  
 [4] H. I. Jørgensen, K. Grove-Rasmussen, T. Novotný, K. Flensberg, and P. E. Lindelof, *Phys. Rev. Lett.* **96**,

- 207003 (2006).
- [5] J. P. Cleuziou, W. Wernsdorfer, V. Bouchiat, T. Ondarcuhu, and M. Monthieux, *Nat. Nanotechnol.* **1**, 53 (2006).
- [6] A. Eichler, R. Deblock, M. Weiss, C. Karrasch, V. Meden, C. Schönenberger, and H. Bouchiat, *Phys. Rev. B* **79**, 161407 (2009).
- [7] J.-D. Pillet, C. H. L. Quay, P. Morfin, C. Bena, A. L. Yeyati, and P. Joyez, *Nat. Phys.* **6**, 965 (2010).
- [8] R. Maurand, T. Meng, E. Bonet, S. Florens, L. Marty, and W. Wernsdorfer, *Phys. Rev. X* **2**, 011009 (2012).
- [9] J. D. Pillet, P. Joyez, R. Žitko, and M. F. Goffman, *Phys. Rev. B* **88**, 045101 (2013).
- [10] J. A. van Dam, Y. V. Nazarov, E. P. A. M. Bakkers, S. De Franceschi, and L. P. Kouwenhoven, *Nature* **442**, 667 (2006).
- [11] E. J. H. Lee, X. Jiang, R. Aguado, G. Katsaros, C. M. Lieber, and S. De Franceschi, *Phys. Rev. Lett.* **109**, 186802 (2012).
- [12] E. J. H. Lee, X. Jiang, R. Žitko, R. Aguado, C. M. Lieber, and S. D. Franceschi, “Scaling of sub-gap excitations in a superconductor-semiconductor nanowire quantum dot,” (2016), arXiv:1609.07582.
- [13] S. Li, N. Kang, P. Caroff, and H. Q. Xu, *Phys. Rev. B* **95**, 014515 (2017).
- [14] A. C. Hewson, *The Kondo Problem to Heavy Fermions*, Cambridge Studies in Magnetism (Cambridge University Press, 1993).
- [15] K. G. Wilson, *Rev. Mod. Phys.* **47**, 773 (1975).
- [16] P. Kopietz, L. Bartosch, and F. Schütz, *Introduction to the functional renormalization group*, Lect. Notes Phys. (Springer-Verlag Berlin Heidelberg, 2010).
- [17] S. Streib, A. Isidori, and P. Kopietz, *Phys. Rev. B* **87**, 201107 (2013).
- [18] K. Edwards, A. C. Hewson, and V. Pandis, *Phys. Rev. B* **87**, 165128 (2013).
- [19] V. Janiš and P. Augustinský, *Phys. Rev. B* **75**, 165108 (2007).
- [20] M. R. Buitelaar, T. Nussbaumer, and C. Schönenberger, *Phys. Rev. Lett.* **89**, 256801 (2002).
- [21] A. Eichler, M. Weiss, S. Oberholzer, C. Schönenberger, A. Levy Yeyati, J. C. Cuevas, and A. Martín-Rodero, *Phys. Rev. Lett.* **99**, 126602 (2007).
- [22] T. Sand-Jespersen, J. Paaske, B. M. Andersen, K. Grove-Rasmussen, H. I. Jørgensen, M. Aagesen, C. B. Sørensen, P. E. Lindelof, K. Flensberg, and J. Nygård, *Phys. Rev. Lett.* **99**, 126603 (2007).
- [23] C. Buizert, A. Oiwa, K. Shibata, K. Hirakawa, and S. Tarucha, *Phys. Rev. Lett.* **99**, 136806 (2007).
- [24] K. Grove-Rasmussen, H. I. Jørgensen, and P. E. Lindelof, *New J. Phys.* **9**, 124 (2007).
- [25] D. J. Luitz, F. F. Assaad, T. Novotný, C. Karrasch, and V. Meden, *Phys. Rev. Lett.* **108**, 227001 (2012).
- [26] A. Martín-Rodero and A. Levy Yeyati, *Adv. Phys.* **60**, 899 (2011).
- [27] V. Meden, *Journal of Physics: Condensed Matter* **31**, 163001 (2019).
- [28] S. De Franceschi, L. Kouwenhoven, C. Schönenberger, and W. Wernsdorfer, *Nat. Nanotechnol.* **5**, 703 (2010).
- [29] H. I. Jørgensen, T. Novotný, K. Grove-Rasmussen, K. Flensberg, and P. E. Lindelof, *Nano Lett.* **7**, 2441 (2007).
- [30] R. Žitko, J. S. Lim, R. López, and R. Aguado, *Phys. Rev. B* **91**, 045441 (2015).
- [31] A. Jellinggaard, K. Grove-Rasmussen, M. H. Madsen, and J. Nygård, *Phys. Rev. B* **94**, 064520 (2016).
- [32] T. Domański, M. Žonda, V. Pokorný, G. Górski, V. Janiš, and T. Novotný, *Physical Review B* **95**, 045104 (2017).
- [33] K. Satori, H. Shiba, O. Sakai, and Y. Shimizu, *J. Phys. Soc. Japan* **61**, 3239 (1992).
- [34] T. Yoshioka and Y. Ohashi, *J. Phys. Soc. Jpn.* **69**, 1812 (2000).
- [35] J.-G. Liu, D. Wang, and Q.-H. Wang, *Phys. Rev. B* **93**, 035102 (2016).
- [36] Y. Tanaka, A. Oguri, and A. C. Hewson, *New J. Phys.* **9**, 115 (2007).
- [37] A. Oguri and Y. Tanaka, *J. Phys.: Conf. Ser.* **391**, 012146 (2012).
- [38] R. Bulla, J. Keller, and T. Pruschke, *Z. Phys. B Condens. Matter* **94**, 195 (1994).
- [39] T. Hecht, A. Weichselbaum, J. von Delft, and R. Bulla, *J. Phys.: Cond. Mat.* **20**, 275213 (2008).
- [40] R. Žitko, “NRG Ljubljana - open source numerical renormalization group code,” (2014), nrgljublana.ijs.si.
- [41] A. K. Mitchell, M. R. Galpin, S. Wilson-Fletcher, D. E. Logan, and R. Bulla, *Phys. Rev. B* **89**, 121105 (2014).
- [42] T. Novotný, A. Rossini, and K. Flensberg, *Phys. Rev. B* **72**, 224502 (2005).
- [43] A. Kadlecová, M. Žonda, and T. Novotný, *Phys. Rev. B* **95**, 195114 (2017).
- [44] H. R. Krishna-murthy, J. W. Wilkins, and K. G. Wilson, *Phys. Rev. B* **21**, 1044 (1980).
- [45] R. Žitko and T. Pruschke, *Phys. Rev. B* **79**, 085106 (2009).
- [46] The broadening has been also predicted analytically in Refs. [32, 52] via the Schrieffer-Wolff transformation. Using the transformation  $\mathbb{T}$ , the  $\Delta \rightarrow \infty$  can be mapped onto the particle-hole asymmetric SIAM, from which the enhancement of the exchange coupling  $J$  compared to the particle-hole symmetric case follows trivially. Thus, as a consequence of the locally induced SC pairing, the  $T_K$  is enhanced and the central peak is broader compared to the single-channel normal SIAM.
- [47] M. Žonda, V. Pokorný, V. Janiš, and T. Novotný, *Sci. Rep.* **5**, 8821 (2015).
- [48] A. Kadlecová, M. Žonda, V. Pokorný, and T. Novotný, *Phys. Rev. Applied* **11**, 044094 (2019).
- [49] P. Seth, I. Krivenko, M. Ferrero, and O. Parcollet, *Comput. Phys. Commun.* **200**, 274 (2016).
- [50] D. J. Luitz and F. F. Assaad, *Phys. Rev. B* **81**, 024509 (2010).
- [51] V. Pokorný and M. Žonda, *Physica B* **536**, 488 (2018).
- [52] T. Domański, I. Weymann, M. Barańska, and G. Górski, *Sci. Rep.* **6**, 23336 (2016).